This paper is a non-peer reviewed preprint submitted to EarthArXiv. It was submitted to the journal Remote Sensing for Environment in July 2023.

Retrieving the irrigation actually applied at district scale: assimilating high-resolution Sentinel-1-derived soil moisture data into a FAO-56-based model

Pierre Laluet[1], Luis Enrique Olivera-Guerra[1,*], Víctor Altés[2,3], Giovanni Paolini[2], Nadia Ouaadi[1,4], Vincent Rivalland[1], Lionel Jarlan[1], Josep Maria Villar[3], Olivier Merlin[1]

[1]Centre d'Etudes Spatiales de la Biosphère (CESBIO), Université de Toulouse, CNES-CNRS-IRD-UPS-INRAE, Toulouse, France

[2]isardSAT, Marie Curie 8-14, Parc Tecnològic Barcelona Activa, Barcelona, Spain

[3]Soils and Water Research group, Universitat de Lleida, Lleida, Spain

[4]GMME/SURFACE, Meteo-France/CNRM, Toulouse, France

*now at: Laboratoire des Sciences du Climat et de l'Environnement, CEA-CNRS-UVSQ-UPSACLAY, UMR 8212, IPSL, Gif-sur-Yvette, France

Correspondence to: pierre.laluet@gmail.com

Abstract

Irrigation is the most water consuming activity in the world. Knowing the timing and amount of irrigation that is actually applied is therefore fundamental for water managers. However, this information is rarely available at all scales and is subject to large uncertainties due to the great diversity of existing agricultural practices and associated irrigation regimes (full irrigation, deficit irrigation, or over irrigation). To fill this gap, we propose a two-step approach based on 15 m resolution Sentinel-1 (S1) surface soil moisture (SSM) data to retrieve the actual irrigation at the weekly scale over an entire irrigation district. As a first step, the S1-derived SSM is assimilated into a FAO-56-based crop water balance model (SAMIR) to retrieve for each crop type both the irrigation amount (I_{dose}) and the soil moisture threshold ($SM_{threshold}$) at which irrigation is triggered. For this, a particle filter method is implemented, with particles reset each month to provide time varying $SM_{threshold}$ and I_{dose}. As a second step, the retrieved $SM_{threshold}$ and I_{dose} values are used as input to SAMIR for estimating the weekly irrigation and its uncertainty. The assimilation approach (SSM-ASSIM) is tested over the 8000 hectare Algerri-Balaguer irrigation district located in north-eastern Spain, where in situ irrigation data integrating the whole district are available at the weekly scale during 2019. For assessment, the performance of SSM-ASSIM is compared against that of the default FAO-56 irrigation module (called FAO56-DEF), which sets $SM_{threshold}$ to the critical soil moisture value and systematically fills the soil reservoir for each irrigation event. During 2019, with a yearly observed irrigation of 687 mm, SSM-ASSIM (FAO56-DEF) shows a Root Mean Square Difference between retrieved and in situ irrigation of 6.7 (17) mm $week^{-1}$, and a Pearson correlation coefficient of 0.88 (0.47). The SSM-ASSIM approach shows great potential for retrieving the weekly water use over extended areas for any irrigation regime, including over irrigation.

Keywords

Irrigation; Assimilation; Soil moisture; Microwave; FAO-56 model; Remote sensing.

1 Introduction

Irrigation is the most water-intensive human activity, consuming over 70% of the freshwater used worldwide (Foley et al., 2011; Qin et al., 2019). Pressure on water resources already exists in many regions and is expected to intensify in the future (Wada et al., 2011, 2013; Campbell et al., 2017; FAO, 2021). This is largely due to the combined effect of increased food demand linked to economic and population growth (Tilman & Clark, 2015), and the impact of climate change on hydrometeorological response (Ferguson et al., 2018; Malek et al., 2018; Williams et al., 2020). To best manage this situation, decision-makers, including water resource managers need to know how much water is being used for irrigation, at regional (irrigation district, catchment), national and global scales (OECD, 2015). However, access to reliable information on irrigation water use is currently lacking. They either do not exist, or are subject to large uncertainties inherent in national or international databases, such as the AQUASTAT dataset (http://www.fao.org/aquastat/en/; accessed 16 June 2023) (Ajaz et al., 2020; Puy et al., 2022a), or in the prediction of hydrological models (Wada et al., 2016; Huang et al., 2018; Puy et al., 2022b). Indeed, models generally simulate irrigation on the basis of empirically defined soil moisture thresholds, which are highly variable in space and time and therefore highly uncertain (Olivera-Guerra et al., 2023). In addition, irrigation modeling is impacted by other sources of uncertainty, such as irrigated area, or irrigation efficiency (Puy et al., 2021, 2022a, 2022b).

While the need for knowledge about irrigation water use is growing, and the irrigation models are still too uncertain to meet the challenge, more and more remote sensing observations relevant to irrigation retrieval are becoming freely available. Over the last two decades, the number of satellites carrying solar and thermal spectrum sensors (e.g., MODIS (Moderate resolution Imaging Spectroradiometer), Landsat, Sentinel-2 (S2), Sentinel-3) from which evapotranspiration (ET) products can be derived (such as SEN-ET; Guzinski et al., 2020), and passive (e.g., SMOS (Soil Moisture and Ocean Salinity), SMAP (Soil Moisture Active Passive) and active microwave (e.g., ASCAT (Advanced SCATterometer), Sentinel-1 (S1)) sensors, from which soil moisture products can be derived (e.g., El Hajj et al., 2017; Ojha et al., 2019; Paolini et al., 2022), has steadily increased. This opens up increasingly interesting possibilities in terms of spatial and temporal resolution (Peng et al., 2021). The wealth of information available through remote sensing led to the emergence of a community of researchers focusing on estimating irrigation from satellite observations. Massari et al. (2021) recently provided an overview of the various existing approaches based on satellite observation. Some of these works have attempted to retrieve irrigation as the difference between simulated and remotely sensed ET (e.g., Anderson et al., 2015; López Valencia et al., 2020) or by comparing remotely sensed ET of two (one irrigated and one rainfed) neighboring crops (e.g., Romaguera et al., 2014; Vogels et al., 2020). However, the information contained in ET is limited to the water actually consumed by plants, thus neglecting any excess of

water applied intentionally (e.g., to allow soil leaching) or unintentionally (due to suboptimal practice) and hence leading to an underestimation of irrigation. Many other recently published approaches propose to estimate irrigation using the surface soil moisture (SSM) data retrieved from microwave observations. Remotely sensed SSM can detect the irrigation signal (Le Page et al., 2020; Jalilvand et al., 2021; Lawston, et al., 2017), and theoretically both under-irrigation (below the amount of water needed to avoid crop stress) and over-irrigation (above the amount of water the soil can hold, resulting in drainage).

An irrigation retrieval model based on SSM data was proposed by Brocca et al. (2018) using the SM2RAIN approach. It has since been used in various works (e.g., Jalilvand et al., 2019; Dari et al., 2020, 2022, 2023; Filippucci et al., 2020). SM2RAIN relies on a simple water balance equation whose terms depend on observed SSM and empirical parameters, which are previously calibrated over rainfed areas or during periods when there is no irrigation. Jalilvand et al. (2019) applied this method using SSM data from the AMSR2 (Advanced Microwave Scanning Radiometer 2; ~25 km resolution) over an irrigation district in Iran. Although the overall irrigation dynamics was well reproduced, irrigation was systematically overestimated. By applying a bias correction obtained from the application of SM2RAIN over rainfed areas, results were significantly improved with a Root Mean Square Deviation (RMSD) of 13 mm month^{-1}. They highlighted the sensitivity of irrigation to the ET formalism and emphasized the need to use SSM observations at higher spatial resolution. Later, Dari et al. (2020) and (2022) applied the same approach on semi-arid irrigation districts in Spain at a finer spatial resolution using the SMOS and SMAP SSM data disaggregated at 1 km resolution (DISPATCH SSM data sets; Merlin et al., 2013). They showed that an improved formulation of ET (notably using the FAO-56 approach of Allen et al., 1998) considerably improves irrigation retrievals. This highlights the importance of properly representing the processes involved in the crop water balance.

Recently, Dari et al. (2023) used SM2RAIN with S1 and CYGNSS (Cyclone Global Navigation Satellite System) derived SSM products (1 km and 6 km spatial resolution, respectively) on ten irrigation districts in Spain, Italy, and Australia. The retrieved irrigation reproduces in situ observations well, but with sometimes significant biases, particularly on small irrigation districts. In fact, all papers involving SM2RAIN have stressed the importance of using a high resolution SSM product to detect processes occurring at the field scale. In parallel with these works, Zappa et al. (2021) proposed an approach close to SM2RAIN based on the comparison of SSM variation between an irrigated pixel and the rainfed pixels surrounding it. Zappa et al. (2022) evaluated the performance of this approach on synthetic data and showed that it is highly sensitive to both spatial resolution and observation frequency. The performance decreases sharply for periods of more than three days between two successive SSM observations, and when the irrigated fraction of a pixel falls below 70%. This illustrates the importance of high-resolution observations, able to provide pixels with a high irrigation fraction.

In addition to the issues of spatial resolution and revisit time of SSM data sets, another limitation of current SSM-based approaches such as SM2RAIN is that they neglect the issue of uncertainty, whether caused by the model (uncertainty in model parameters and formalism) or by satellite observations (uncertainty in input data).

Yet, all models are sensitive to the choices made in the calibration step, to the model formalism and parameterization, and to the uncertainty of its input data (Foster et al., 2020; Beven et al., 2019; Puy et al., 2022b). Knowledge of the uncertainty in the model estimate is actually as important as the modeled value to provide reliable information to decision-makers and managers (Saltelli et al., 2020).

Other approaches based on the assimilation of satellite SSM data into land surface models (LSM) have recently been developed, enabling uncertainty to be taken into account in irrigation simulations. Assimilation methods are based on the prior distribution of both model and observation errors. Felfelani et al. (2018) assimilated SMAP (36 km spatial resolution) SSM data into the Community Land Model version-4.5 LSM (Lawrence et al., 2011; Oleson et al., 2013) over a large irrigated area in the USA, using the one-dimensional Kalman filter method. The objective was to constrain the so-called "target soil moisture" parameter, which governs the irrigation triggering and amount. They obtained a significant improvement in simulated irrigation compared to the baseline simulation performed using the default parameter value. Also, their results were considerably better when a bias correction derived from numerous in situ SSM measurements was applied to the SMAP SSM data. In the same vein, Abolafia-Rosenzweig et al. (2019) inverted irrigation quantities by assimilating (synthetic) SSM data into the variable infiltration capacity LSM using the particle batch smoother data assimilation approach. Results of the twin experiment indicated that the assimilation approach is better when the timing of irrigation is known, and when the revisit time of SSM observation is shorter than three days. They also highlighted the importance of tackling the issue of persistent biases between simulated and observed SSM. Jalilvand et al. (2023) applied the same approach but using the 1 km resolution SMAP-S1 SSM data (Das et al., 2019) over an irrigation district in Iran. They confirmed the importance of an a priori knowledge of irrigation frequencies in their approach and obtained an underestimation of seasonal cumulative irrigation at the irrigated pixels by an average of 19%, explained by the loss of irrigation signal due to the mismatch between the spatial resolution (1 km) of SSM data and the scale of irrigation practices. They also showed that performance was not significantly affected by increasing error in the assimilated SSM.

Modanesi et al. (2022) assimilated the S1 backscatter (aggregated to 1 km resolution) to improve the performance of the Noah-MP.v.3.6 LSM (Niu et al., 2011) coupled with an irrigation module (Ozdogan et al., 2010a), using an ensemble Kalman filter. The assimilation resulted in an improvement of the simulated irrigation, but to a limited extent. Especially, they stressed the importance of dealing with observations and simulations at higher spatial resolution (with poorer performances when irrigation fraction was low), as well as the need for more frequent SSM observations and improving the Noah-MP.v.3.6 irrigation module formalism. At a finer spatial scale, Ouaadi et al. (2021) estimated the timing and quantities of irrigation of five wheat plots in Morocco. They assimilated a high-resolution (15 m, revisit time of six days) SSM product derived from S1 into a model based on the FAO-56 method, using the particle filter (PF) approach (Vrugt et al., 2013). PF is one of the most efficient assimilation methods, able to take into account model and observation uncertainties without the need for any assumptions on prior density functions or likelihoods and is adapted to non-linear problems (unlike 4DVar or Kalman filter-based methods) (van Leeuwen et al., 2019; Alonso-

González et al., 2022). For all five plots, Ouaadi et al. (2021) obtained a Pearson correlation coefficient r of 0.64 and an RMSD of 28.7 mm/15 days and succeeded in detecting 50-70% of irrigation events. They also showed, using in situ data, that their approach performed better with a shorter revisit time (three days).

A recurring issue in assimilation approaches is the management of persistent differences between modeled and observed SSM. To reduce model or observation biases, one possible solution is to use a rescaling approach such as cumulative distribution function matching (Reichle and Koster., 2004) to fit the observed SSM to the simulated SSM. However, this approach has the disadvantage of potentially deleting signals when the observations contain some information that is not modeled, such as irrigation (Kumar et al., 2015; Nair and Indu, 2019). Another way to minimize such a bias is to calibrate model parameters on rainfed pixels (e.g., Dari et al., 2020, 2022; Jalilvand et al., 2023), although this implies the strong (and unverified) assumption that optimal parameters for rainfed pixels are also optimal for irrigated pixels. Another approach is to remove a systematic bias (calculated on rainfed pixels) from the simulated irrigations (Jalilvand et al., 2019), although part of the signal may be lost due to the difference in climatology or soil properties between both pixel types (Brombacher et al., 2022).

The above literature review of SSM-based irrigation retrieval methods indicates that state-of-the-art approaches are currently limited by (one or several of the following factors): 1) the coarse resolution of SSM remote sensing products used as input, 2) the impact of data gaps in SSM time series due to low revisit, 3) the non-explicit representation of irrigation-related (e.g. ET, deep percolation, etc.) processes which makes the calibration steps difficult and uncertain, and 4) the lack of consideration (by the irrigation retrieval methods that are not based on data assimilation) of uncertainties in both model parameterization and input data.

In this context, this study proposes a new assimilation scheme of a high (15 m) resolution S1-derived SSM product (Ouaadi et al., 2020) into the FAO-56-based crop water balance model SAtellite Monitoring for IRrigation (SAMIR; Simonneaux et al., 2009), using the PF method. The SAMIR model implemented at the field scale allows for a robust and explicit representation of crop ET from the crop coefficient values available for all common crops for various climates in the FAO-56 look up tables. It is hence spatializable over large extents from readily available data (Laluet et al., 2023b). Moreover, the assimilation approach developed by Olivera-Guerra et al. (2023) is used here to invert two parameters of the SAMIR irrigation module: the irrigation amount (I_{dose}) and the soil moisture threshold ($SM_{threshold}$) at which irrigation is triggered. Both parameters are retrieved over successive monthly assimilation windows integrating several (up to five independent) S1-derived SSM observations. Such a strategy helps reduce the impact of possible data gaps in SSM time series and allows for representing weekly district-scale water uses in any (deficit, full or excess) irrigation regimes (Olivera-Guerra et al., 2023).

The proposed approach is implemented over the 8000 hectare Algerri-Balaguer (AB) irrigation district located in north-eastern Spain. It is evaluated at the field and AB scales using in situ irrigation measurements available at both scales. The paper is organized as follows: Section 2 presents the study area and the data used, Section

3 presents the SAMIR model and its irrigation module (Section 3.1), as well as the assimilation scheme (Section 3.2), the strategy for performing plot-scale simulations (Section 3.3), and the evaluation step (Section 3.4). Section 4 presents and discusses the results first obtained at the field scale using in situ SSM data as input (Section 4.1), then at the AB district scale using S1-derived SSM data as input (Section 4.2). Section 5 provides conclusions and perspectives of this work.

2 Study area and data

2.1 Study area

The study area is the 8000 hectare Algerri-Balaguer (AB) irrigation district located in the north east of Spain, 20 km north of the city of Lleida. The climate is continental Mediterranean with an average annual reference evapotranspiration (ET_0) of 1027 mm and rainfall of 380 mm (2000-2021). For the year 2019, 6140 hectares were irrigated, of which 94% were covered by five main crop types: double crops (62% of the irrigated area; mainly barley or wheat in winter-spring season and maize in summer-fall), summer cereals (9%; maize), winter cereals (8%; mainly barley or wheat), forages (8%; mainly alfalfa), and fruit trees (7%). The remaining 6% are composed of leguminous, oleaginous, horticultural and protein crops, as well as vineyards and olive trees. All plots are irrigated by sprinkler (in summer the daily doses range from 5 to 15 mm), except for the fruit trees being irrigated with drip irrigation system. The land use information used in this study comes from the Geographic Information System for Agricultural Parcels (SIGPAC), provided by the Department of Climate Action, Food, and Rural Agenda of the Region of Catalonia, and is available at https://agricultura.gencat.cat/ca/ambits/desenvolupamentrural/sigpac/descarregues (accessed 16 June 2023). Figure 1.a shows the AB district with the land cover for the year 2019 from the SIGPAC database.

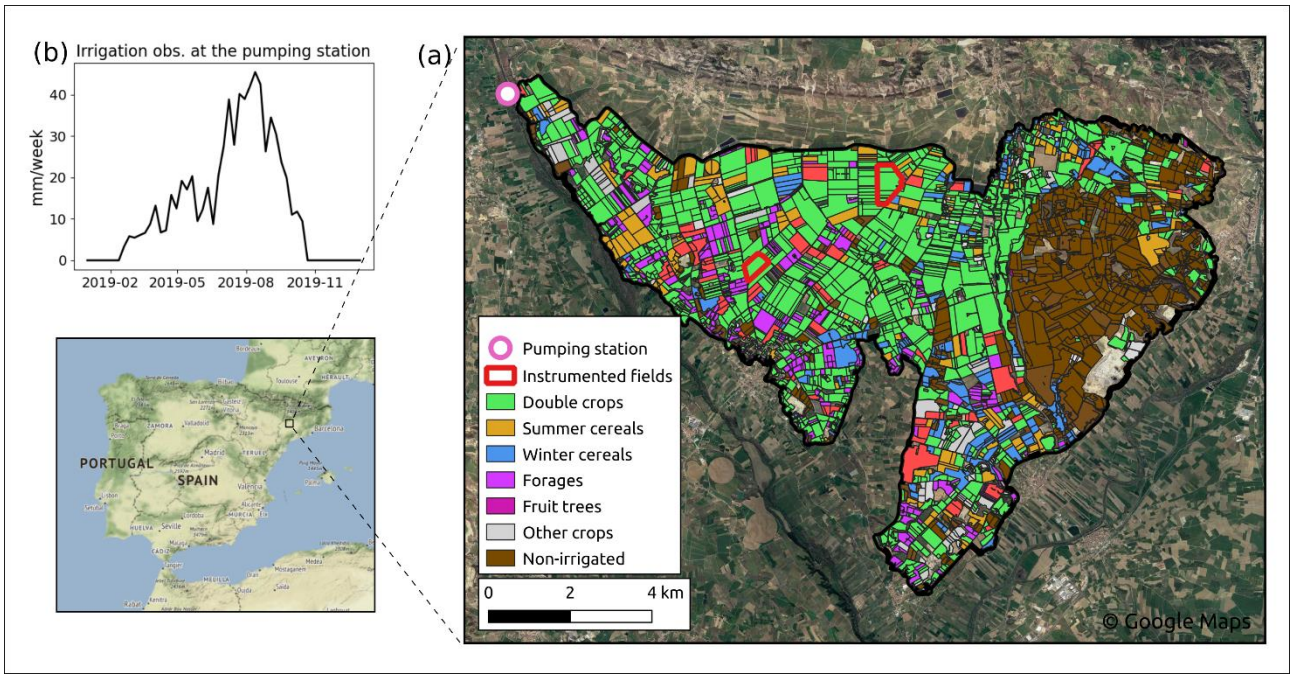

Figure 1: The AB irrigation district with the land cover for the year 2019, the location of the pumping station and of the two instrumented plots (Albesa and Castello) (a), and the weekly irrigation data measured at the pumping station in 2019 (b) (coordinates: 797157/4636983.4 ETRS89/UTM zone 31N).

2.2 In situ data

2.2.1 District-scale in situ irrigation data

The district-scale irrigation data consists of the water flow pumped in the river Noguera Ribagorçana just next to the AB area (cf. Figure 1.a for the location of the pumping station) used exclusively for the irrigation of AB and being its only resource. Flow measurements have been made on a daily basis by the SAIH (Automatic Hydrological Information System of the Ebro Basin; available at http://www.saihebro.com/saihebro/index.php; accessed 16 June 2023), and were aggregated to a weekly basis to account for the time lag between pumping and actual irrigation (Olivera-Guerra et al., 2023). In addition, 5.8% of the pumped volume is removed to account for evaporative losses and leakage, based on a comparison made in 2021 between the yearly water pumped and the yearly irrigation measured with flowmeters at the district level (Olivera-Guerra et al., 2023). In situ weekly irrigation data for the year 2019 are shown in Figure 1.b.

2.2.2 Field-scale in situ data

The instrumented fields Castello and Albesa are two double-cropped plots of 35 and 21 hectares respectively, located in the AB district (cf. Figure 1.a for the location of the two instrumented fields). At Castello, SSM data every 15 minutes are available for a five-month period in summer-fall 2021. At Albesa, SSM data every 15 minutes are available for three periods: six months in summer-fall 2021, five months in winter-spring 2022, and five months in summer-fall 2022. For Castello, SSM data are obtained from the average of SSM measurements from two TEROS 10 sensors (METER group) installed at a depth of 5 cm and separated by a distance of 100 m. For Albesa, they are derived from three sensors (two TEROS 10 and one EC-5; METER group) also about 100 m apart. For the periods mentioned, daily irrigation data from flowmeters are available at both Castello and Albesa fields. These in situ data are used to test and evaluate the SSM-ASSIM approach on a simple case (crop type and irrigation practices spatially uniform), at the plot scale, and with in situ SSM data being more frequent and less prone to error than satellite observations. The in situ SSM measurements were averaged on a daily basis and one day out of three were kept, resulting in an observation every three days. This provides a frequency higher than that of S1-derived SSM (the latter being six days), but low enough to mimic satellite observation frequencies (2-3 days being the frequency of SMOS or SMAP).

2.2.3 In situ meteorological data

The meteorological data are obtained from five stations belonging to the Catalan meteorological station network (available at https://ruralcat.gencat.cat/agrometeo.estacions; accessed 16 June 2023). Two of them are located within the AB district, and three at a maximum distance of 5 km. The average standard deviation of both precipitation and ET_0 measurements made by the five stations is very low. Therefore, their spatial average were used as forcing in the SAMIR model.

2.3 Remote sensing data

2.3.1 S2-derived vegetation index

Normalized Difference Vegetation Index (NDVI) is used in this study to drive the modeled development of crops in SAMIR. It is derived from the S2 multispectral satellite constellation made of two satellites S2A and S2B, with a 5-day global revisit frequency. S2A and S2B were launched by the European Space Agency (ESA) in 2015 and 2017, respectively. We used the level 2 surface reflectance data at 10 m spatial resolution from band 4 (red) and band 8 (near-infrared) to compute NDVI, and cloud masks (QA60 and band 10) were applied. When more than 25% of the pixels falling in a plot are affected by the cloud masks, all the pixels of this plot are removed to avoid cloud contamination. When less than 25% of the plot is affected by the masks, the average of the remaining NDVI values within the crop field is calculated. Finally, the field-scale NDVI data is interpolated to the daily scale using a piecewise cubic Hermite interpolation polynomial method (Fritsch and Carlson, 1980).

2.3.2 S1-derived SSM

The remotely sensed SSM data used in this study are derived from the S1 C-band synthetic aperture radar satellite constellation, consisting of two satellites S1A and S1B, with a global revisit frequency of six days. S1A and S1B were launched by ESA in 2014 and 2016, respectively, and both provide dual acquisitions in VV (vertically transmitted, vertically received) and VH (vertically transmitted, horizontally received) polarizations. To invert the SSM from S1 microwaves observations, the approach proposed by Ouaadi et al. (2020) is used. The retrieval method is based on the inversion of the Water Cloud model from the S1 VV polarization backscatter coefficient and the S1 interferometric coherence. The vegetation descriptor used in the Water Cloud model is the above ground biomass derived from the interferometric coherence. SSM is hence obtained at each S1 acquisition and for each pixel by minimizing the distance between the backscatter coefficient observed by S1 and the one simulated by the Water Cloud model, using a "brute-force" approach. For more details on the S1-derived SSM product, the reader can refer to the original paper by Ouaadi et al. (2020).

2.4 Ancillary soil data

The soil texture is relatively uniform over AB and corresponds to a silty clay soil (Jahn et al., 2006). It is derived from the SoilGrids product (available at https://maps.isric.org; accessed 15 May 2023) at 250 m resolution (Hengl et al., 2017; Poggio et al., 2021). Soil texture information is used in SAMIR to derive hydraulic soil properties, which control the volume of water the soil can hold and the evaporation dynamics of the surface soil layer.

3 Method

The overall methodology to retrieve the weekly irrigation at the district scale is presented in the flowchart of Figure 2. The SAMIR model is first described with its irrigation module (3.1). Then, the SSM-ASSIM approach to retrieve the daily irrigation parameters ($SM_{threshold}$ and I_{dose}) (3.2.1), and the strategy to simulate the weekly irrigation using the retrieved $SM_{threshold}$ and I_{dose} as input parameters in SAMIR are presented (3.2.2). Finally, the strategy to apply the SSM-ASSIM approach at plot scale (section 3.3), and for evaluating irrigation retrievals at both field and district scales (section 3.4) are described.

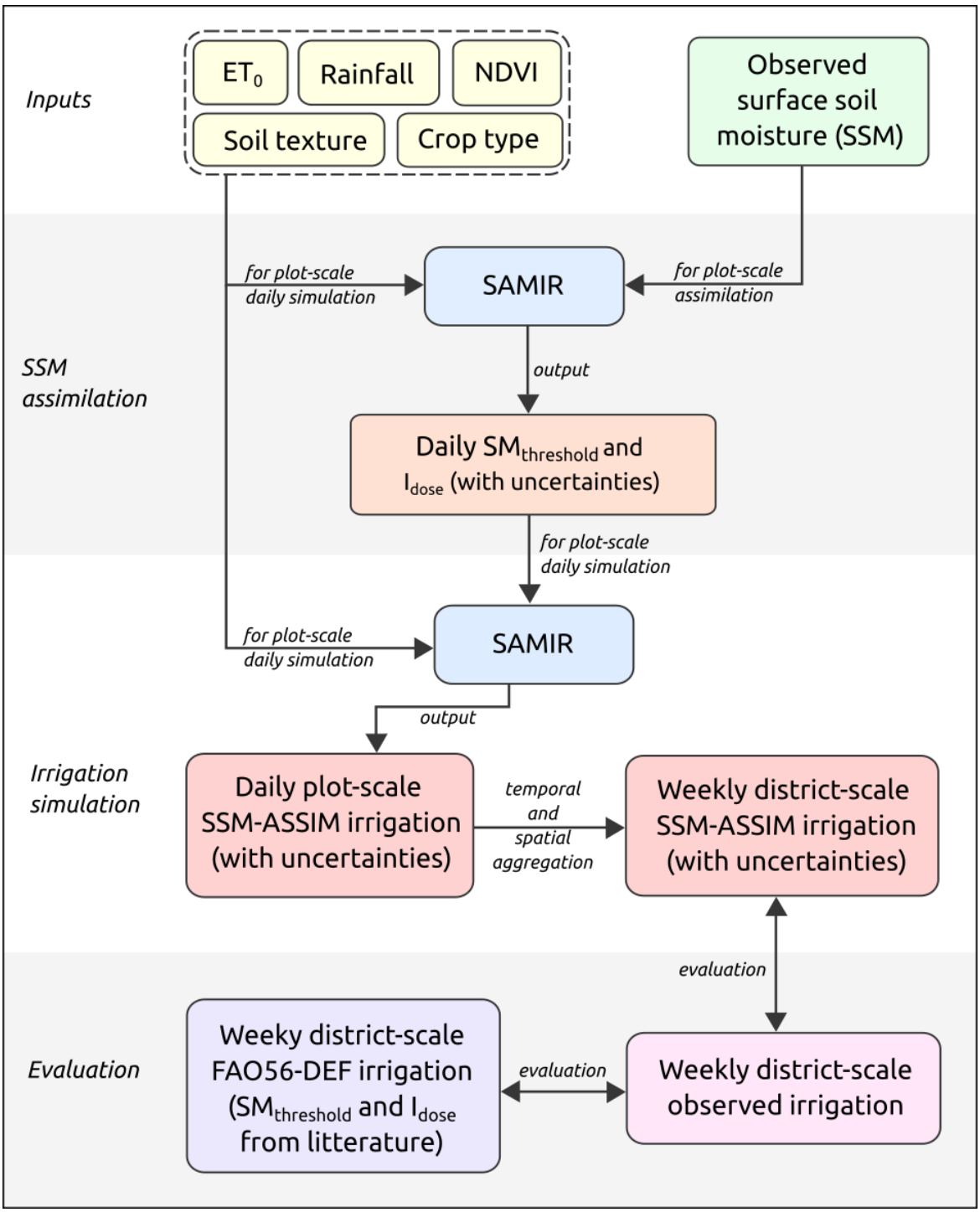

Figure 2: Flowchart of the methodology to retrieve the weekly irrigation at district scale by assimilating SSM data into the SAMIR model.

3.1 SAMIR model

SAMIR is a FAO-56 double-crop coefficient-based model (Allen et al., 1998) originally designed to simulate the crop water balance components for estimating daily ET and optimal irrigation needs, by considering the water status of plant and soil. It uses meteorological forcing variables to calculate ET_0 (using the Penman-Monteith equation), precipitation, crop and soil parameters, and NDVI to drive plant development.

3.1.1 SAMIR main equations

SAMIR simulates the daily water balance equation as:

$$Dr(t) = Dr(t-1) + ET(t) - P(t) - I(t) + DP(t) \quad (1)$$

where Dr is the root zone depletion, ET the actual evapotranspiration, P the precipitation, I the irrigation and DP the deep percolation. Each term is expressed in mm for day t (and t-1 for Dr), and ET is obtained by multiplying two crop coefficients to ET_0 as follows:

$$ET(t) = [Kcb(t) \cdot Ks(t) + Ke(t) \cdot Kr(t)] \cdot ET_0(t) \quad (2)$$

where $ET_0 \cdot Kcb \cdot Ks$ is the water transpired by plants (T, mm), and $ET_0 \cdot Ke \cdot Kr$ the soil evaporation (E, mm). Kcb (-) is the basal crop coefficient controlling potential crop transpiration, computed from a linear relationship with NDVI, Ks (-) is the crop water stress coefficient reducing potential transpiration, Ke (-) is the potential soil evaporation coefficient and Kr (-) is the evaporation reduction coefficient.

The calculation of Ks is based on the daily water balance calculation in the root zone layer, and can be written as:

$$Ks(t) = \frac{TAW(t) - Dr(t)}{TAW(t)(1-p)} \quad (3)$$

where Dr is calculated from the daily water balance according to Eq. (1), and TAW (mm) is the total (maximum) available water in the root zone. p is a crop-specific parameter provided in the literature (Allen et al., 1998; Pereira et al., 2021), ranging between 0.4 and 0.6 for most crops and being corrected daily for weather conditions. Allen et al. (1998) suggest that p controls the water depth threshold below which irrigation should be triggered to avoid crop water stress (and irrigate optimally) by keeping Dr below $TAW \cdot p$. In other words, p triggers irrigation when soil moisture reaches a critical level (below which the crop experiences water stress) called $SM_{critical}$, provided in the literature. p can then be written as follows:

$$p = 1 - \left(\frac{SM_{critical} - SM_{WP}}{SM_{FC} - SM_{WP}}\right) \quad (4)$$

where SM_{FC} ($m^3 m^{-3}$) is the soil moisture at field capacity and SM_{WP} ($m^3 m^{-3}$) the soil moisture at wilting point, which are both derived from soil texture using the pedotransfer function proposed by Román-Dobarco et al. (2019). In the AB district, SM_{FC} and SM_{WP} are fairly homogeneous with values of 0.330 (± 0.005) $m^3 m^{-3}$ and 0.207 (± 0.006) $m^3 m^{-3}$, respectively. For the Castello instrumented plot, SM_{FC} and SM_{WP} derived from SoilGrid are 0.339 $m^3 m^{-3}$ and 0.186 $m^3 m^{-3}$, respectively, and for Albesa 0.336 $m^3 m^{-3}$ and 0.191 $m^3 m^{-3}$.

Olivera-Guerra et al. (2023) proposed an alternative to the p parameter for triggering irrigation, which is $p_{trigger}$. Unlike p, $p_{trigger}$ does not trigger irrigation when $SM_{critical}$ is reached, but when $SM_{threshold}$ is. $SM_{threshold}$ is time-

varying and can be different from $SM_{critical}$, allowing to reproduce farmers' current practices. $p_{trigger}$ is written as follows:

$$p_{trigger}(t) = 1 - \left(\frac{SM_{threshold}(t) - SM_{WP}}{SM_{FC} - SM_{WP}}\right) \quad (5)$$

TAW of Eq. (3) is computed as follows:

$$TAW(t) = (SM_{FC} - SM_{WP}) \cdot Zr(t) \quad (6)$$

where Zr (mm) is the rooting depth, varying between a minimum value (set at 100 mm for annual crops) and a crop-dependent maximum value (reached at the maximum NDVI of the simulated field).

Kr, the evaporation reduction coefficient is written as follow:

$$Kr(t) = \left[0.5 - 0.5 \cdot cos\left(\frac{\pi \cdot SSM(t)}{SM_{saturation}}\right)\right]^{P} \quad (7)$$

where $SM_{saturation}$ is the soil moisture at saturation derived from the soil texture using a pedotranfer function, and P is a semi-empirical parameter also derived from the soil texture (Amazirh et al., 2021; Merlin et al., 2016). As SSM is not explicitly represented in SAMIR, it is derived from the surface soil water depletion (De, mm), the total (maximum) evaporable water (TEW, mm), and the soil evaporation layer depth (Ze, fixed at 150 mm), as follows:

$$SSM(t) = 0.5 \cdot SM_{WP} + \left(\frac{TEW - De(t)}{Ze}\right) \quad (8)$$

With TEW being calculated as follows:

$$TEW = (SM_{FC} - 0.5 \cdot SM_{WP}) \cdot Ze \quad (9)$$

3.1.2 Default irrigation simulation with SAMIR (FAO56-DEF approach)

SAMIR simulates irrigation using two irrigation parameters: $SM_{threshold}$ and I_{dose}. $SM_{threshold}$ is the soil moisture level at which irrigation is automatically triggered and is used to calculate $p_{trigger}$ (see Eq. 5). I_{dose} is the irrigation dose applied when irrigation is triggered. By default, SAMIR uses $SM_{threshold}$ and I_{dose} values producing a theoretically optimal irrigation regime. We call this default irrigation mode FAO56-DEF. In the FAO56-DEF approach, irrigation is triggered when $SM_{threshold}$ equals $SM_{critical}$ (see Eq. 5) and I_{dose} is calculated as the volume of water required to fill the reservoir completely, without exceeding SM_{FC}. With this approach, as soon as the simulated soil moisture reaches $SM_{critical}$, irrigation is triggered, thus avoiding crop water stress. Excess irrigation (generating drainage loss) is also avoided as I_{dose} fills the root reservoir up to the SM_{FC} and not beyond.

3.1.3 Irrigation simulation in any irrigation regime with SAMIR

To represent real agricultural practices and associated irrigation regimes, Olivera-Guerra et al. (2023) proposed a time-varying $SM_{threshold}$ and I_{dose} able to simulate actual irrigation. With time-varying values different from those used by FAO56-DEF, it is possible to simulate temporally-varying irrigation water use in any (optimal, deficit or even over) irrigation regime. When $SM_{threshold}$ is lower than $SM_{critical}$, this corresponds to a deficit irrigation regime, whereas when it is higher, it corresponds to an over irrigation regime. Figure 3 illustrates for a theoretical double-cropped plot, the relative difference between $SM_{threshold}$ values for an ideal ($SM_{threshold}$ set at $SM_{critical}$) and real (time-varying $SM_{threshold}$) case. The green line represents the ideal case triggering irrigation at the onset of crop water stress (FAO56-DEF approach). The red line represents the theoretical real case, with a variable $SM_{threshold}$ (for example inverted from SSM data). We use herein the term "real case" as opposed to "ideal case" but note that the variable $SM_{threshold}$ of Figure 3 is theoretical and does not correspond to a real experiment. In Figure 3, $SM_{threshold}$ values below $SM_{critical}$ in winter-spring would result in a deficit irrigation regime (cf. red shaded area), as the theoretical irrigator waits for the soil moisture level to be low before irrigating. Conversely, $SM_{threshold}$ values above $SM_{critical}$ in summer-fall lead to excessive irrigation (cf. blue area), as the theoretical irrigator irrigates while the soil moisture is still high.

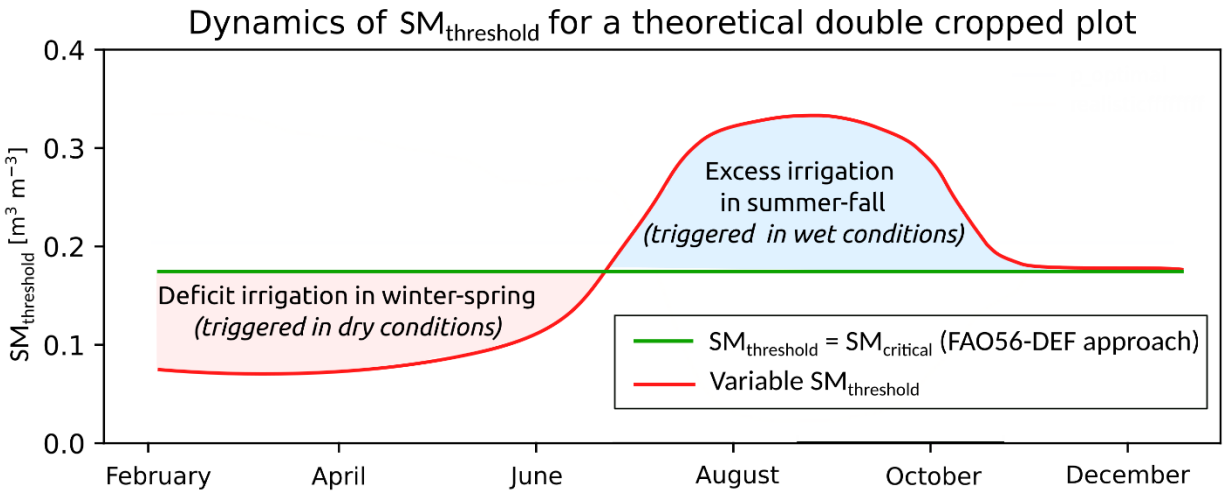

Figure 3: Schematic dynamics of $SM_{threshold}$ for a theoretical double cropped plot for an ideal (FAO56-DEF; green line) and real (red line) case. The red shaded area represents deficit irrigation due to $SM_{threshold}$ values lower than $SM_{critical}$ (during winter-spring in this theoretical example), and the blue shaded area shows excess irrigation due to $SM_{threshold}$ values larger than $SM_{critical}$ (during summer-fall in this theoretical example).

3.2 Retrieving irrigation from the assimilation of SSM observations (SSM-ASSIM)

3.2.1 Inverting $SM_{threshold}$ and I_{dose} parameters

To retrieve variable $SM_{threshold}$ and I_{dose}, SSM observations are assimilated into SAMIR using the PF method. The first step of the PF method consists of randomly drawing N initial samples (particles) having different parameter values. In our case, 300 particles with different ($SM_{threshold}$, I_{dose}) pairs are generated following a uniform distribution between SM_{WP} and SM_{FC} for $SM_{threshold}$, and between 0 and 20 mm d^{-1} for I_{dose}. Next, simulations are performed for each particle and for each day, until an observation is available (every six days for S1-derived SSM, every three days for in situ SSM). On the day of the SSM observation, the N simulated variables (here the 300 SSM simulated by SAMIR) are confronted with the observation. During this evaluation step, each particle ($SM_{threshold}$ and I_{dose} pairs, resulting in SSM simulation) is assigned a weight according to its likelihood with the observed SSM. The best particles are duplicated a number of times relative to their likelihood, and the worst ones are discarded.

In order to calculate the weight of the particles, and also to prevent their degeneracy, the PF method considers the model and observations errors. For the observed SSM errors, a standard deviation of 20% of the observed SSM value is set for both S1-derived SSM and in situ SSM, this value being in line with the errors of the existing SSM satellite products (Das et al., 2019; Kerr et al., 2010). For the model error, a standard deviation of 10% of the parameter value is applied to the three most sensitive SAMIR parameters (two parameters related to the NDVI-Kcb relationship and Zr_{max}; Laluet et al., 2023a), as well as to the surface and root compartment depletions (De and Dr). To avoid as much as possible the degeneracy of particles, their weights are reset whenever the effective sample size N_{eff} reaches a threshold of one third of the initial particle size number (more details in Moradkhani et al., 2005; van Leeuwen et al., 2019).

In addition, the 300 particles are reset to their initial values every 30 days, i.e., every five successive S1-derived SSM observations and ten in situ SSM observations. This results in monthly mean and standard deviation $SM_{threshold}$ and I_{dose} values computed with the particle weights obtained at the end of the month. The monthly timescale allows accounting for changes in irrigation regime throughout the year, while ensuring a certain number of observations needed for the PF method to converge with satisfying uncertainty. In order to get smoother $SM_{threshold}$ and I_{dose} values, the whole assimilation scheme is then repeated five times, shifting the starting date by six days each time. Subsequently, $SM_{threshold}$ and I_{dose} are obtained on a daily basis (mean and standard deviation) by averaging the five time series of monthly retrieved $SM_{threshold}$ and I_{dose}. Figure 4 shows a flowchart describing the PF-based approach used in this study.

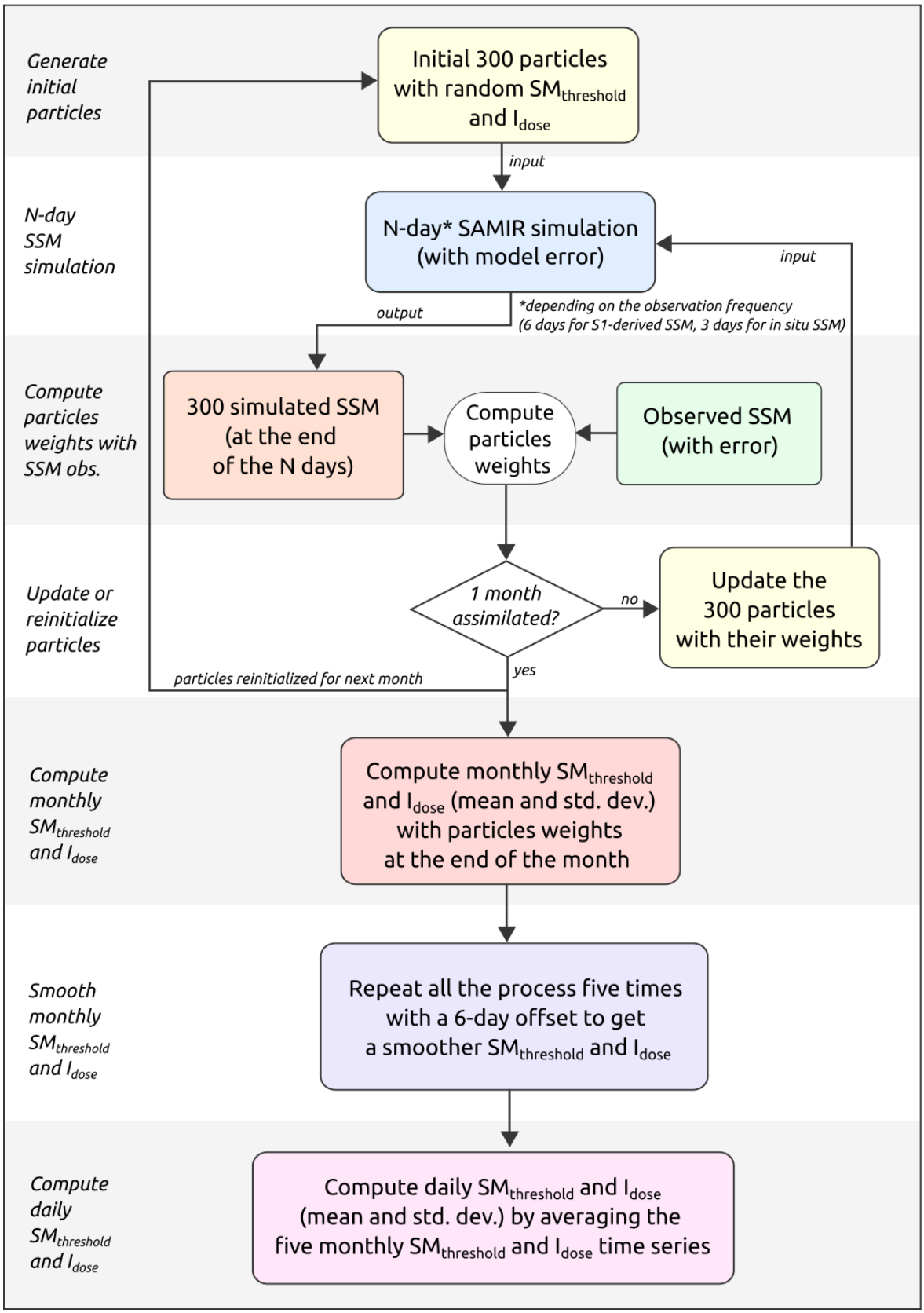

Figure 4: Flowchart of the PF-based assimilation approach of SSM data into SAMIR every six days for S1-derived SSM (every three days for in situ SSM), within 1-month periods.

3.2.2 Simulating irrigation from the retrieved $SM_{threshold}$ and I_{dose} parameters

Once daily $SM_{threshold}$ and I_{dose} have been retrieved with the PF-based assimilation approach, they are used as input in SAMIR to simulate irrigation. For this, 1000 time series of $SM_{threshold}$ and I_{dose} are randomly sampled following a normal distribution with their retrieved daily mean and standard deviation, and are then used as input parameters in SAMIR to simulate 1000 time series of daily irrigation. Daily irrigations are then aggregated at the weekly scale, and the mean and standard deviation of weekly irrigation are obtained from the 1000 simulated weekly irrigation time series.

3.3 Aggregation at the crop type scale

To simplify our approach as much as possible, and to minimize its computational cost, we selected the five main crop types (double crops, summer cereals, winter cereals, forages, and fruit trees) representing 94% of the irrigated area in 2019, and computed the average of their input (NDVI, SSM, and soil texture) weighted by their total surface area. Five average plots representing 94 % of the irrigated part of AB are thus obtained. The remaining 6% are represented by the average of the five main crop types. Averaging the plots by crop type is justified by the fact that the soil texture is fairly homogeneous over the area (in addition to having a low sensitivity in SAMIR; Laluet et al., 2023a). Figure 5 shows the mean and standard deviation of the S1-derived SSM and the S2-derived NDVI time series for the five average plots. The dynamics of NDVI and SSM time series observed for plots that belong to a given crop type are not strongly scattered (Figure 5) reflecting homogeneity in terms of farming practices (sowing date, irrigation practices). At the end of the SSM-ASSIM process, the simulated irrigations for each of the five average plots are averaged and weighted by their total surface area within AB to obtain an irrigation amount representative of the entire AB district.

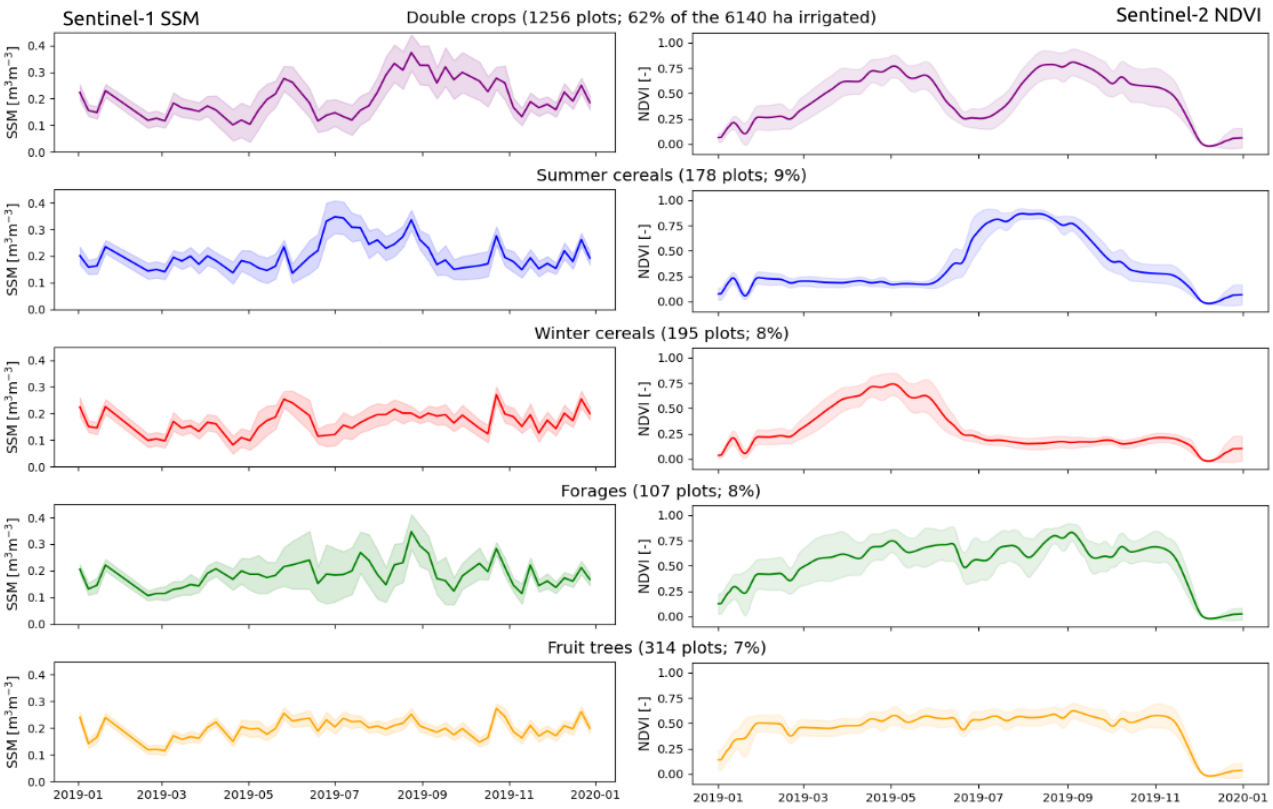

Figure 5: Mean and standard deviation of S1-derived SSM (left) and S2-derived NDVI (right) for each of the five main crop types for 2019.

3.4 Evaluation of retrieved irrigation

The Root Mean Square Deviation (RMSD), the Pearson correlation coefficient (r), and the bias between retrieved and in situ weekly irrigation are calculated. At the district scale this is done for both SSM-ASSIM and FAO56-DEF approaches, and the uncertainty simulated with SSM-ASSIM is assessed. At plot level, only SSM-ASSIM is evaluated.

4 Results and discussion

In this section we first present the irrigation results obtained by applying the SSM-ASSIM approach at the scale of the Albesa and Castello plots, using in situ SSM data every three days for assimilation (Section 4.1). Then, the irrigation results obtained with the SSM-ASSIM and the FAO56-DEF approaches at the district scale using S1-derived SSM data are presented and discussed (4.2.1). Finally, the results of the SSM-ASSIM approach are put into perspective with other works (4.2.2), and limitations and perspectives are highlighted (4.2.3).

4.1 Field-scale experiment using in situ SSM

This section aims to assess the SSM-ASSIM performance at the field scale where the crop type and irrigation practices can be considered spatially uniform. In situ SSM data from the Albesa and Castello double cropped fields are used. Figure 6 shows the results for the two plots and the four periods studied: Castello summer-fall 2021 (a), Albesa summer-fall 2021 (b), Albesa winter-spring 2022 (c), and Albesa summer-fall 2022 (d). Each plot shows, in addition to rainfall, the in situ SSM (purple line), the $SM_{threshold}$ (dark blue line) and the I_{dose} (light blue line) retrieved with SSM-ASSIM, and the simulated irrigation using the retrieved $SM_{threshold}$ and I_{dose} as forcing in SAMIR (green line) along with the observed irrigation (black line). Standard deviation of the input SSM data set (used for assimilation; 20% of the observed value), $SM_{threshold}$, I_{dose} and simulated irrigation are shown. Bias and RMSD values are given in the chart titles. Note that no bias correction between simulated and observed SSM was applied.

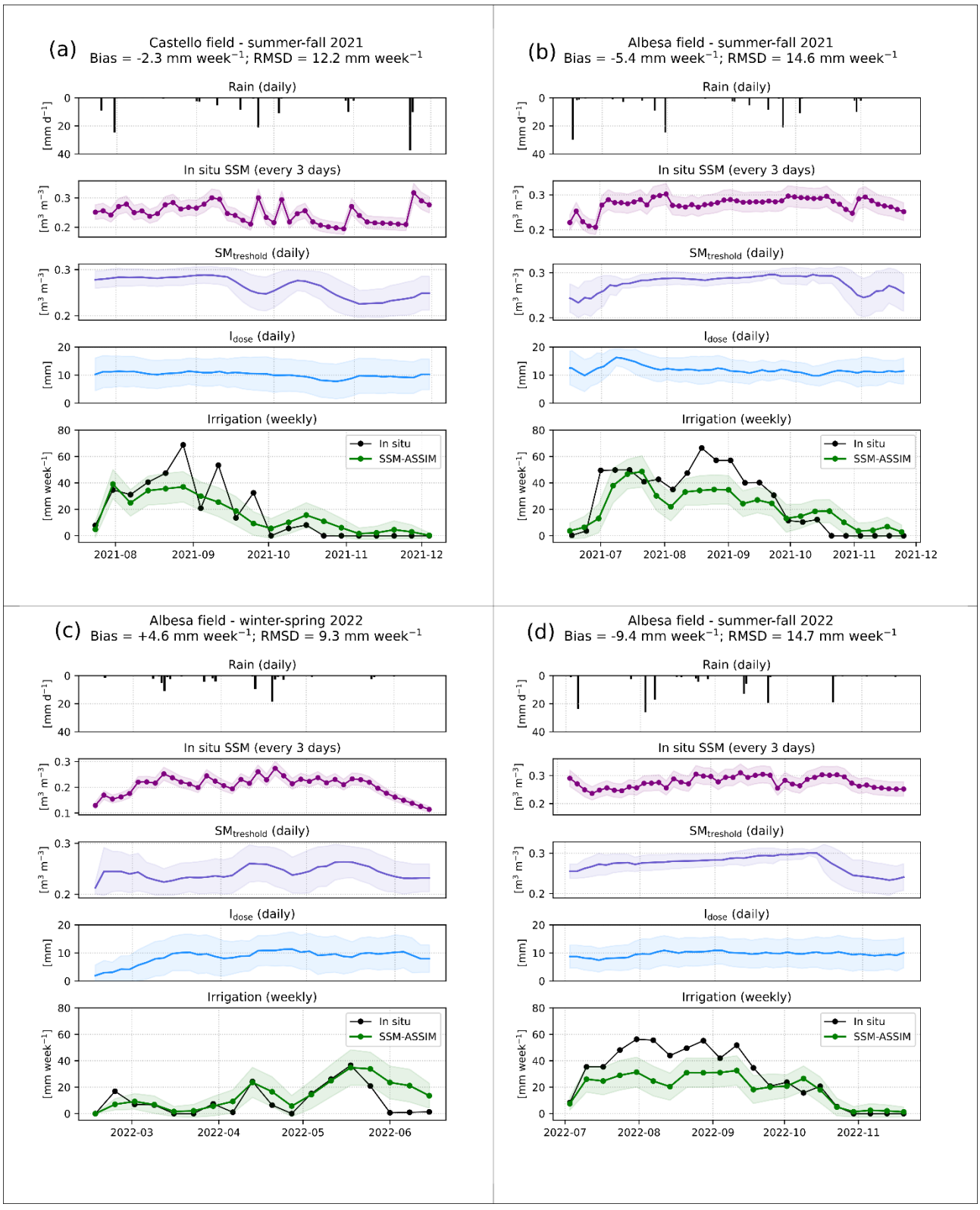

Figure 6: Daily rain (black bars), in situ SSM every three days (purple line), daily $SM_{threshold}$ (dark blue line), daily I_{dose} (light blue line), and weekly irrigation retrieved with the SSM-ASSIM approach (green line) and weekly in situ irrigation (black line), for Castello summer-fall 2021 (a), Albesa summer-fall 2021 (b), Albesa winter-spring 2022 (c), and Albesa summer-fall 2022 (d) separately.

Figure 6 should be read as follows: the assimilation of in situ SSM data in SAMIR results in a daily $SM_{threshold}$ and a daily I_{dose} which, given as forcing to SAMIR, provides the irrigation retrieved by the SSM-ASSIM approach. For example, in Figure 6.b we can observe that, at the start of the season, the relatively low in situ SSM values (around 0.20 m^3 m^{-3}) suddenly rise to around 0.28 m^3 m^{-3} when the irrigation season begins. This results in a retrieved $SM_{threshold}$ that increases rapidly from 0.23 to 0.27 m^3 m^{-3}, and an I_{dose} that rises from around 10 mm d^{-1} to over 15 mm d^{-1}, when the irrigation season begins. By using these $SM_{threshold}$ and I_{dose} pairs as forcing in SAMIR, the simulated irrigation reproduces pretty well the start of the irrigation season.

Figure 6 shows that our approach correctly reproduces the irrigation start and end dates for each season. It also indicates that SSM-ASSIM slightly overestimates irrigation during the winter-spring season (mostly in June; Figure 6.c), while it underestimates it during the three summer-fall seasons (Figs. 6.a, 6.b, and 6.d). This results in a bias of +4.6 mm $week^{-1}$ for Albesa winter-spring 2022, -2.3 mm $week^{-1}$ for Castello summer-fall 2021, -5.4 mm $week^{-1}$ for Albesa summer-fall 2021, and -9.4 mm $week^{-1}$ for Albesa summer-fall 2022. The RMSD for Albesa winter-spring 2022 is 9.3 mm $week^{-1}$, while it is slightly larger for Castello summer-fall 2021 (12.2 mm $week^{-1}$), Albesa summer-fall 2021 (14.6 mm $week^{-1}$) and Albesa summer-fall 2022 (14.7 mm $week^{-1}$). Note that the irrigation amounts are much larger during summer-fall (between 40 and 70 mm $week^{-1}$ for the most intensive irrigation period in August-September) than during the winter-spring season (between 0 and 40 mm $week^{-1}$), hence explaining the larger RMSD values obtained in summer-fall.

For the three summer-fall seasons, SSM-ASSIM generally underestimates irrigation (-12% for Castello summer-fall 2021, -20% for Albesa summer-fall 2021, and -32% for Albesa summer-fall 2022). For these three seasons, simulated weekly irrigation never exceeds 50 mm $week^{-1}$. During the most intensive irrigation period weekly simulated irrigation is generally between 25 and 40 mm $week^{-1}$, whereas observed irrigation is between 40 and 60 mm $week^{-1}$. This means that the weekly simulated irrigation is, although too low, sufficient for the simulated SSM to match the observed SSM. Indeed, $SM_{threshold}$ and I_{dose} are inverted from the observed SSM. Therefore, if more irrigation would have been needed to better match simulated and observed SSM, the inverted $SM_{threshold}$ during intensive irrigation seasons would have been larger (to trigger more frequent irrigation events), as well as the inverted I_{dose} (to irrigate with a larger water amount). We hypothesize that one of the reasons for this is the non-linearity in the relationship between SSM and irrigation. Let's consider a farmer irrigating heavily a field with sprinklers (e.g., 10 mm d^{-1}). During the first hour of irrigation, the SSM can vary rapidly from low (dry soil) to high values (wet soil). As the irrigation event continues, the water applied will generate a weaker response in terms of SSM variation than at the start of irrigation, due in particular to infiltration into the underlying soil layer. This is illustrated in Figure 6, where we can see that the underestimation in summer occurs generally when the in situ SSM is at high values, close to SM_{FC} (~0.34 m^3 m^{-3}).

4.2 District-scale experiment using satellite SSM

4.2.1 Evaluation of the SSM-ASSIM and FAO56-DEF approaches

Figure 7 shows the retrieved weekly irrigation at AB in 2019 with SSM-ASSIM (green line) and FAO56-DEF (orange line), together with in situ irrigation data (black line). SSM-ASSIM reproduces fairly well the beginning and end of irrigation seasons, as well as general irrigation dynamics (RMSD of 6.7 mm week^{-1} and r of 0.88; Table 1). In contrast, FAO56-DEF does not reproduce the observed irrigation dynamics (RMSD of 16.7 mm week^{-1}, and r of 0.47), as it simulates few irrigation events with large doses. In terms of bias over the whole year 2019, SSM-ASSIM (+0.3 mm week^{-1}) is slightly better than FAO56-DEF (-0.6 mm week^{-1}). Cumulative in situ irrigation for 2019 is 687 mm year^{-1}, while that simulated by SSM-ASSIM is 706 mm year^{-1} (+19 mm year^{-1}), and 654 mm year^{-1} (-33 mm year^{-1}) by FAO56-DEF. Note that, as with the field experiment, no bias correction between simulated SSM and observed S1-derived SSM was applied.

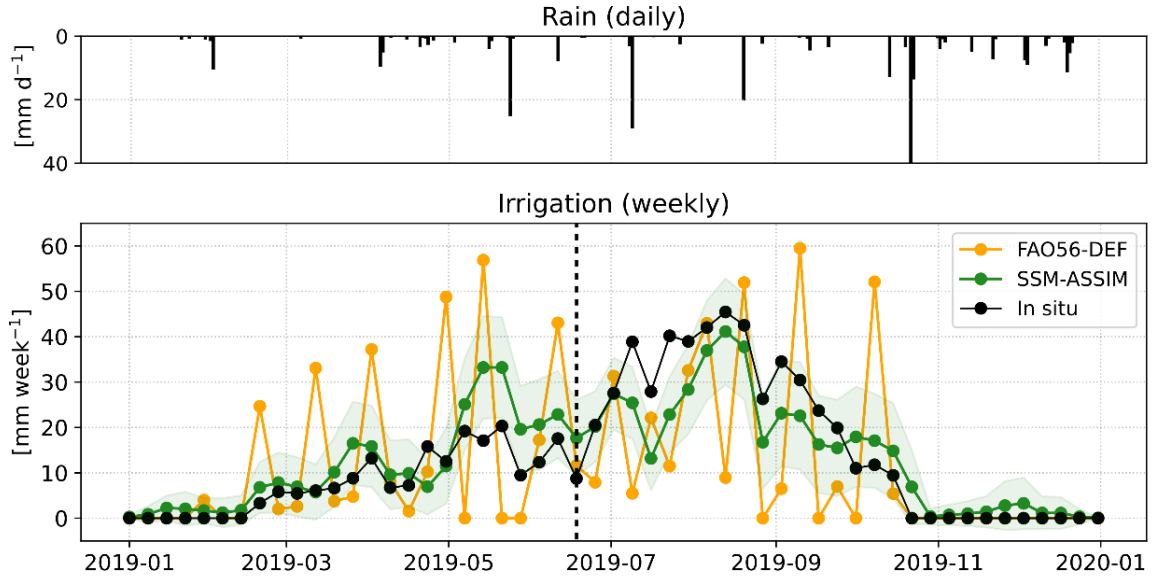

Figure 7: Top: daily rainfall at AB. Below: weekly irrigation simulated at the AB scale with the SSM-ASSIM approach (green line), with the FAO56-DEF approach (orange line), and observed irrigation (black line), for 2019. The vertical dotted line divides the winter-spring and summer-fall irrigation seasons.

Table 1: RMSD, bias, and r between retrieved and in situ irrigation for SSM-ASSIM and FAO56-DEF at the AB scale for 2019, as well as for the winter-spring and the summer-fall seasons separately.

	SSM-ASSIM			FAO56-DEF		
	RMSD [mm week^{-1}]	Bias [mm week^{-1}]	r [-]	RMSD [mm week^{-1}]	Bias [mm week^{-1}]	r [-]
All 2019	6.7	+0.3	0.88	16.7	-0.6	0.47
Winter-spring [01/01/2019 to 18/06/2019]	6.2	+3.7	0.89	15.9	+4.5	0.47
Summer-fall [19/06/2019 to 31/12/2019]	7.1	-2.6	0.94	17.3	-5.2	0.56

In line with the results for the field-scale experiment using in situ data (Section 4.1), SSM-ASSIM underestimates irrigation for the summer-fall period (bias of -2.6 mm week^{-1}). However, the underestimation in summer at the district scale is less marked than for the field scale experiment (Albesa summer-fall 2021 has a bias of -5.4 mm week^{-1} and Albesa summer-fall 2021 of -9.4 mm week^{-1}). In contrast to the latter, at the AB district scale, SSM-ASSIM is able to simulate summer irrigation values close to observed maxima (41 mm week^{-1} simulated mid-August 2019, for an in situ irrigation of 46 mm week^{-1}; cf. Figure 7). This may be due to the lower observed irrigation during the intense irrigation period in summer at AB scale (around 40 mm week^{-1}) where there are different types of crops, compared to Albesa and Castello fields (around 50 to 60 mm week^{-1}) where there is only maize. Consequently, the limitation mentioned in Section 4.1 regarding the difficulty of simulating high weekly irrigation amounts, even with high observed SSM values, is less of a problem at the AB scale. This suggests that the SSM-ASSIM approach is particularly suited to the district scale: different types of crops with different irrigation regimes are considered together at the district scale, and the weighted (by crop type) average of observed irrigation is lower in summer than on highly irrigated (100 % maize) plots such as Albesa and Castello.

SSM-ASSIM tends to overestimate irrigation during the winter-spring season (bias of +3.7 mm week^{-1}), consistent with the field scale results (Section 4.1). While for the months of January to April, irrigation quantities and dynamics are well reproduced, an overestimation occurs in May-June. To understand why, Figure 8 shows the time series of precipitation (a), S1-derived SSM (b), as well as the retrieved $SM_{threshold}$ (c), I_{dose} (d), and irrigation (e) with SSM-ASSIM for the main crop type (double crop) in the area. From May to mid-June 2019, S1-derived SSM detects irrigation, with SSM rising from 0.11 m^3 m^{-3} at the beginning of May to 0.28 m^3 m^{-3} at the end of May. This large difference in SSM generates a significant increase of both retrieved $SM_{threshold}$ and I_{dose}, leading to important weekly irrigation in May for the double crop plots, which in turn led to an overestimation of irrigation at AB scale at that time. In fact, moments of strong SSM growth correspond

to those when simulated irrigation is largest. Furthermore, although the average weekly irrigation simulated for all AB with SSM-ASSIM performs satisfactorily, the associated uncertainty is significant (±53%, 706 ± 375 mm year^{-1}; shaded green area in Figure 7).

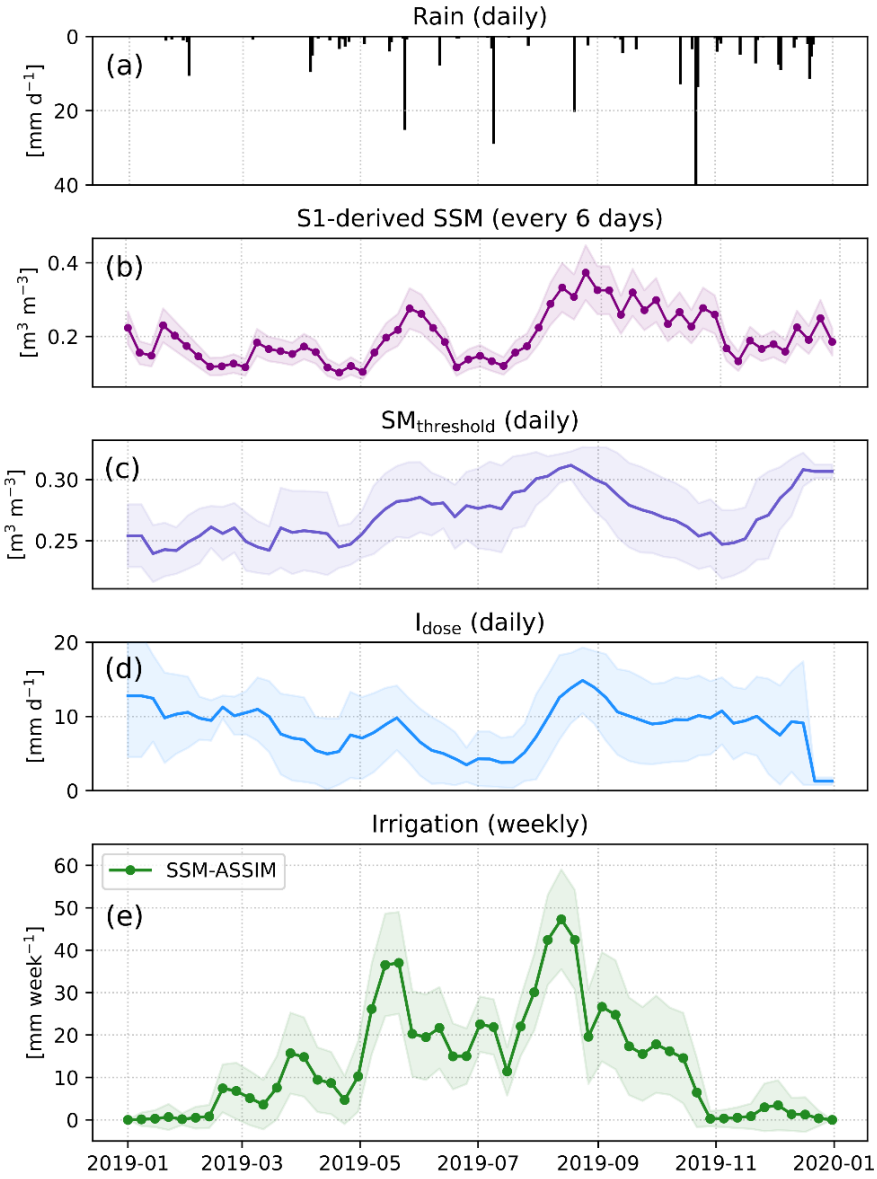

Figure 8: For double crop plots: daily rain (black bars) (a), S1-derived SSM (purple line) (b), $SM_{threshold}$ (dark blue line) (c), I_{dose} (light blue line) (d), and irrigation (green line) retrieved with SSM-ASSIM (e).

4.2.2 Comparison with SSM-ASSIM results from other works

This section aims to put the results obtained with SSM-ASSIM into perspective, by comparing them with other results obtained on the same irrigated district using a different approach. The latter is that proposed by Dari et al. (2023) which, to our knowledge, is to date the only work to have addressed the estimation of irrigation from satellite-based SSM data on the AB district for the year 2019 (their study covers the years 2016 to 2019). This

comparison is made possible thanks to the fact that Dari et al. (2023) made available the weekly irrigation they simulated at the 1 km pixel scale for several irrigation districts, including AB (https://zenodo.org/record/7341284; accessed 20 June 2023).

Dari et al. (2023) used an approach based on the SM2RAIN algorithm, already described in the introduction (Section 1), which is considerably different from SSM-ASSIM, in particular because of its simpler formalism that depends strongly on observed SSM data and on empirical parameters requiring calibration. The spatial resolution of the S1-derived SSM product they use is 1 km, and so are the irrigation simulations. In contrast, our approach is based on a finer scale simulation of crop water consumption, considering model and observation errors. Moreover, SSM-ASSIM uses an S1-derived SSM product with a 15 m resolution.

It is important to note that for this comparison, the in situ irrigation data used for validation differ from that used by Dari et al. (2023). Indeed, in this study, irrigation in mm is obtained by dividing the data by the surface area actually irrigated in 2019 as reported by SIGPAC (61.4 km²), whereas Dari et al. (2023) did so on the basis of the surface area equipped with irrigation systems (70.9 km²). In addition, Dari et al. (2023) removed 10% of the irrigation data in order to consider losses, whereas we only removed 5.8% as explained in Section 2.2.1. This leads to a +17% difference between in situ irrigation used in this study (687 mm $year^{-1}$) and the one used by Dari et al. (2023) (569 mm $year^{-1}$).

Figure 9 shows for the year 2019 the weekly irrigation obtained with SM2RAIN (red line), the one obtained with SSM-ASSIM (green line), and the in situ irrigation (black line). Although both approaches are able to capture the irrigation signal, SM2RAIN underperforms SSM-ASSIM, with a general underestimation of irrigation and an RMSD of 11.6 mm $week^{-1}$ (6.7 mm $week^{-1}$ for SSM-ASSIM), a bias of -5.0 mm $week^{-1}$ (+0.3 mm $week^{-1}$), and an r of 0.65 (and 0.88) for the year 2019 (Table 2). While SM2RAIN manages to reproduce relatively well the dynamics at the start of the 2019 summer-fall irrigation season in July, it significantly underestimates irrigation during the months of August and September, when irrigation is particularly intense (Figure 9).

Table 2: RMSD, bias, and r between retrieved and in situ irrigation for SM2RAIN and SSM-ASSIM at the AB scale for all 2019.

	RMSD [mm $week^{-1}$]	Bias [mm $week^{-1}$]	r [-]
SM2RAIN (Dari et al., 2023)	11.6	-5.0	0.65
SSM-ASSIM	6.7	+0.3	0.88

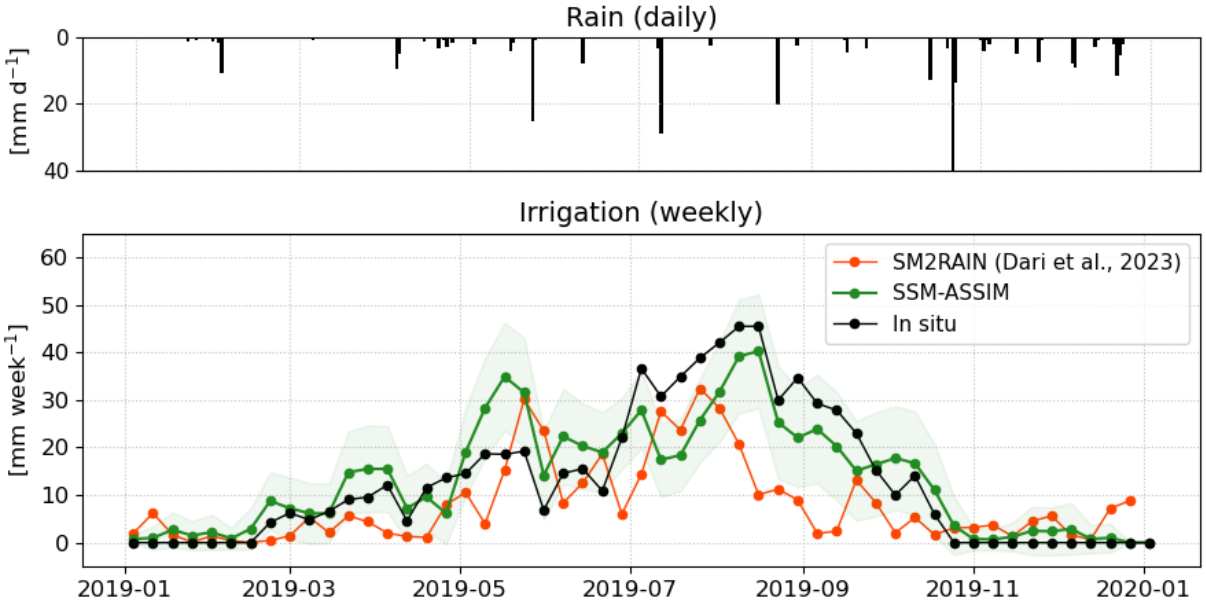

Figure 9: Top: daily rainfall in AB. Below: weekly irrigation simulated at the AB scale with the SM2RAIN approach (Dari et al., 2023) (red line), with the SSM-ASSIM approach (green line), and observed irrigation (black line), for 2019.

Such differences in terms of performance may be the consequence of certain features of the SSM-ASSIM approach. In particular, we think that the implementation of the approach on a plot scale –allowing the plot-level processes governing plant consumption to be captured– is key to simulate irrigation dynamics. This plot-scale approach is made possible by the quality and the fine spatial resolution of the S1-derived SSM product used in this study, which provides a distinct SSM signature and thus an irrigation signature for each plot.

4.2.3 Quality of S1-derived SSM product and its impact on the SSM-ASSIM irrigation retrieval

Figure 7 shows that most of the irrigation underestimation with the SSM-ASSIM approach using S1-derived SSM occurs in July (at the start of the summer-fall irrigation season). We believe that these underestimates are related to the difficulty of the S1-derived SSM product in detecting the actual SSM at the start of the second irrigation season (when vegetation is poorly developed) for double crop fields.

This assumption is supported by two elements:

1) Figure 8.b shows low S1-derived SSM values for double crop plots in late June and early July, at the start of the summer-fall irrigation season. However, in situ irrigation at the AB scale (black line Figure 7) shows that the summer irrigation season has already started by then. There is a difference of about one month between the start of the summer-fall irrigation season at AB scale and the increase in S1-derived SSM for the double crop plots. Yet we would expect the re-analyzed SSM to increase more

rapidly after the start of the irrigation season, as the double crop plots represent 62% of the AB irrigated surface.

2) At the plot level, the time delay between the first irrigation events of the second growing season and the first significant increase in S1-derived SSM is also observed. Figure 10.a shows rainfall (black bar) and in situ irrigation (orange area) for the summer-fall 2021 season at the Albesa instrumented plot. Figure 10.b shows the daily in situ SSM (red line) and the S1-derived SSM (blue line) for the same plot. Note that in situ and S1-derived SSM have been normalized between their minimum and maximum values to facilitate their comparison. It appears that when the irrigation season starts at the end of June, in situ SSM increases almost instantaneously, while S1-derived SSM starts to increase one month later, around the end of July.

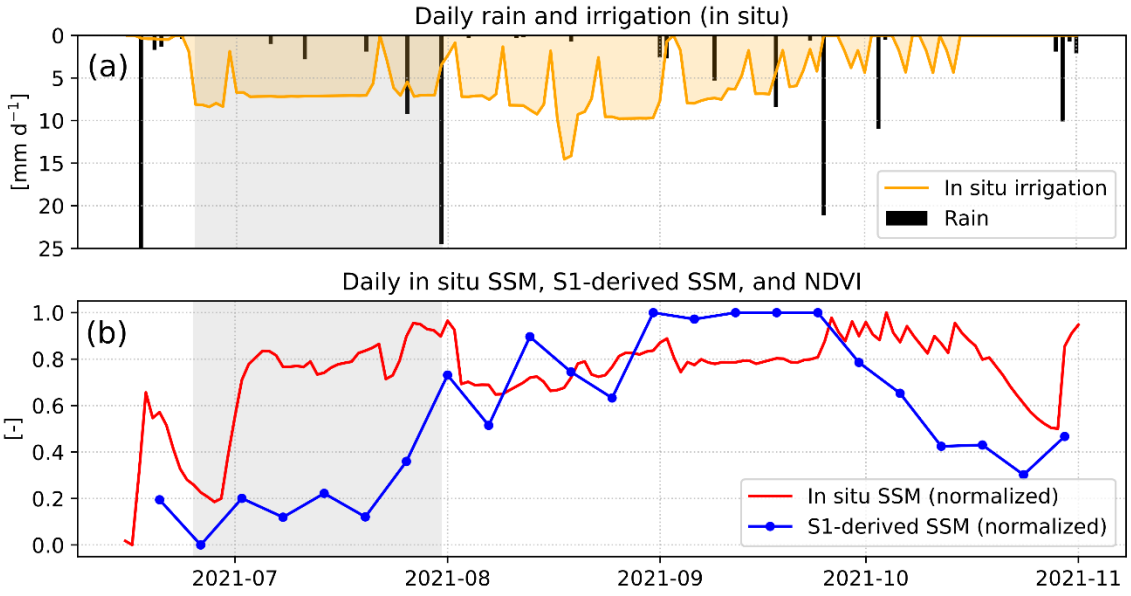

Figure 10: For the Albesa (21 hectares) double crop plot: daily in situ rain (black bars) and irrigation (orange line) (a), daily in situ SSM (red line) and S1-derived SSM every six days (blue line) normalized between their minimum and maximum values (b), for the period from June 2021 to November 2021.

Figure A1 was added to the appendix to explain why low S1-derived SSM values are observed at the beginning of the summer season over the double crop fields. Figure A1 shows time series of S1 backscattering coefficient, S1-derived interferometric coherence (used as vegetation descriptor), S1-derived SSM and S2-derived NDVI (related to the vegetation development) over the Albesa field for 2019. During the inter-crop period in early summer, the maximum of coherence is 0.6 while it is above 0.7 in winter (as in Ouaadi et al., 2021; Santoro et al., 2010). This low level of interferometric coherence in early summer indicates that the scatterer structure is different between the winter and summer inter-seasons. This is probably because in AB, maize is sown directly without tillage in summer, leaving the soil partially covered (unlike in winter) by the remaining stalks. Yet,

the relationship between coherence and above-ground biomass used in the inversion process is calibrated on the assumption that the growing season starts with bare soil (and therefore with a coherence value assumed to be above 0.7). With a coherence of 0.6 observed in AB during early summer, a bias appears in the SSM retrieved at this moment. This is explained by the fact that the radiative transfer model used for the inversion process reaches the observed level of backscatter with the contribution of the canopy only with dry soil underneath. Furthermore, this phenomenon seems to occur only in the case of double plot crops; other crop types with a single crop per year (winter cereals and summer cereals) don't seem to be affected by this issue.

Identifying this difficulty in detecting SSM in early summer (when two crops are grown consecutively in the same year) in the SSM inversion algorithm proposed by Ouaadi et al. (2020) represents an important avenue for improving the quality of S1-derived SSM on double crop fields, and consequently the performance of the SSM-ASSIM approach. With a higher S1-derived SSM value at the start of the summer irrigation season, more irrigation would be retrieved by SSM-ASSIM, thus reducing the summer underestimation issue, and improving the assimilation performance.

5 Summary and conclusion

In a context of increasing pressure on water resources, managers and decision-makers need to know how much water is used for irrigation. Yet there is a lack of reliable information on these quantities, at all spatial scales. To meet this need, a growing number of studies proposed approaches combining models and satellite observations, particularly of SSM. Although encouraging results have been obtained, state-of-the-art SSM-based irrigation retrieval methods have been limited by the spatio-temporal resolution of available SSM data, and the difficulty of representing irrigation-related processes over large areas, and of explicitly taking into account uncertainties in irrigation estimates.

To fill the gap, we propose a new approach (SSM-ASSIM) to assimilate high-spatial-resolution (15 m) SSM data into the FAO-56-based SAMIR model at the plot scale using a PF assimilation method, addressing the above-mentioned challenges. The output of SSM-ASSIM is the mean and standard deviation of two smoothed monthly parameters of the SAMIR irrigation module, namely $SM_{threshold}$ and I_{dose}, governing the irrigation triggering and dose, respectively. The retrieved irrigation and its uncertainty are obtained at weekly scale by running SAMIR with the retrieved distribution of $SM_{threshold}$ and I_{dose} as forcing. For validation, the approach is applied to two instrumented fields for which in situ SSM and irrigation data are available, and to the 8000 ha AB irrigation district where in situ irrigation data are available. At the district scale, irrigation is also simulated with the FAO-56 default configuration (FAO56-DEF) as a benchmark to assess the performance of SSM-ASSIM.

Results at the plot scale using in situ SSM data show that SSM-ASSIM reproduces very well the irrigation dynamics across the agricultural season. However, an underestimation occurs during periods of intense irrigation for the three summer-fall seasons. This can be explained by the large quantities of irrigation applied

to these plots in summer, which as they exceed ~50 mm week^{-1} are not fully captured in the SSM signal. A slight overestimation is also observed for the winter-spring season. When applied at the district scale using S1-derived SSM data, SSM-ASSIM clearly outperforms FAO56-DEF and can reproduce the observed weekly irrigation fairly well, with an r of 0.88 and an RMSD of 6.7 mm week^{-1} for the year 2019. However, as with field-scale experiments, SSM-ASSIM tends to overestimate irrigation in winter-spring (bias of +3.7 mm week^{-1}) and underestimate it in summer-fall (-2.6 mm week^{-1}). The overestimation in winter-spring is related to the discrepancy between very low SSM values at the start of the season followed by a sudden rise in SSM (observed for the double crops representing 62% of the AB area), resulting in high levels of simulated irrigation. The underestimation in summer is attributed to the degraded quality of the S1-derived SSM in early summer for double crop plots.

The performance of SSM-ASSIM relies on the quality of the SSM product. Any improvement in the accuracy and precision of SSM estimates at the field scale would therefore enhance the quality of irrigation retrievals. In addition, the relationship between SSM and irrigation is highly nonlinear due to the shallow depth (~0-5 cm) sensed by microwave sensors. The saturation of SSM sensitivity to large irrigation amounts is an intrinsic limitation of SSM-based assimilation approaches. This problem could eventually be solved by the joint assimilation of thermal-derived ET data which, in hydric stress conditions, are directly linked to the soil moisture accumulated in the root zone. This prospect is all the more encouraging as new thermal missions will soon be launched with LSTM (Land Surface Temperature Monitoring; Koetz et al., 2018) and TRISHNA (Thermal infraRed Imaging Satellite for High-resolution Natural resource Assessment; Lagouarde et al., 2018), offering in the near-future ET and crop stress index products with an unprecedented high spatial and temporal resolution. Finally, the SSM-ASSIM approach could be integrated in large scale LSM to take more realistically account of irrigation and its impact on the hydrological cycle.

Funding

This study was supported by the IDEWA project (ANR-19-P026-003) of the Partnership for research and innovation in the Mediterranean area (PRIMA) program and by the Horizon 2020 ACCWA project (grant agreement # 823965) in the context of the Marie Sklodowska-Curie research and innovation staff exchange (RISE) program.

CRediT authorship contribution statement

Pierre Laluet: Conceptualization, Methodology, Software, Validation, Formal analysis, Investigation, Visualization, Writing – original draft. **Luis Enrique Olivera-Guerra**: Conceptualization, Methodology, Software, Writing – review & editing. **Víctor Altés**: Data curation, Writing – review & editing. **Giovanni Paolini**: Data curation, Writing – review & editing. **Nadia Ouaadi**: Methodology, Visualization, Writing –

review & editing. **Vincent Rivalland**: Software, Writing – review & editing. **Lionel Jarlan**: Methodology, Writing – review & editing. **Josep Maria Villar**: Data curation, Writing – review & editing, Supervision. **Olivier Merlin**: Conceptualization, Methodology, Validation, Writing – review & editing, Supervision.

Declaration of Competing Interest

The authors declare that they have no competing interests.

Acknowledgments

The authors would like to thank the Comunitat de Regants Canal Algerri Balaguer and the Automatic Hydrological Information System of the Ebro Basin for providing the irrigation observation data used in this study. We also want to thank Eric Chavanon (CESBIO) and Jérémy Auclair (CESBIO) who helped optimize the SAMIR code.

Appendix

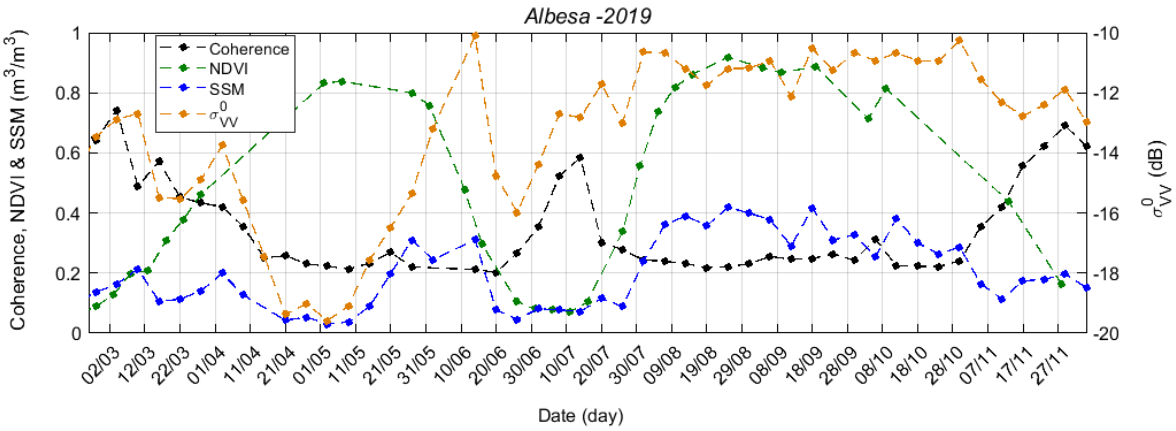

Figure A1: Time series of the S1 backscattering coefficient at VV polarization ($\boldsymbol{\sigma^0_{VV}}$) (orange line), S1-derived interferometric coherence (black line), S2-derived NDVI (green line) and S1-derived SSM (blue line) over Albesa field for 2019.

References

Abolafia-Rosenzweig, R., Livneh, B., Small, E. e., Kumar, S. v., 2019. Soil Moisture Data Assimilation to Estimate Irrigation Water Use. Journal of Advances in Modeling Earth Systems 11, 3670–3690. https://doi.org/10.1029/2019MS001797

Ajaz, A., Datta, S., Stoodley, S., 2020. High Plains Aquifer–State of Affairs of Irrigated Agriculture and Role of Irrigation in the Sustainability Paradigm. Sustainability 12, 3714. https://doi.org/10.3390/su12093714

Allen, R., Pereira, L., Smith, M., 1998. Crop evapotranspiration-Guidelines for computing crop water requirements-FAO Irrigation and drainage paper 56.

Alonso-González, E., Aalstad, K., Baba, M.W., Revuelto, J., López-Moreno, J.I., Fiddes, J., Essery, R., Gascoin, S., 2022. The Multiple Snow Data Assimilation System (MuSA v1.0). Geoscientific Model Development 15, 9127–9155. https://doi.org/10.5194/gmd-15-9127-2022

Amazirh, A., Merlin, O., Er-Raki, S., Bouras, E., Chehbouni, A., 2021. Implementing a new texture-based soil evaporation reduction coefficient in the FAO dual crop coefficient method. Agricultural Water Management 250, 106827. https://doi.org/10.1016/j.agwat.2021.106827

Anderson, R.G., Lo, M.-H., Swenson, S., Famiglietti, J.S., Tang, Q., Skaggs, T.H., Lin, Y.-H., Wu, R.-J., 2015. Using satellite-based estimates of evapotranspiration and groundwater changes to determine anthropogenic water fluxes in land surface models. Geoscientific Model Development 8, 3021–3031. https://doi.org/10.5194/gmd-8-3021-2015

Beven, K., 2019. Towards a methodology for testing models as hypotheses in the inexact sciences. Proc Math Phys Eng Sci 475, 20180862. https://doi.org/10.1098/rspa.2018.0862

Brocca, L., Tarpanelli, A., Filippucci, P., Dorigo, W., Zaussinger, F., Gruber, A., Fernández-Prieto, D., 2018. How much water is used for irrigation? A new approach exploiting coarse resolution satellite soil moisture products. International Journal of Applied Earth Observation and Geoinformation 73, 752–766. https://doi.org/10.1016/j.jag.2018.08.023

Brombacher, J., Silva, I.R. de O., Degen, J., Pelgrum, H., 2022. A novel evapotranspiration based irrigation quantification method using the hydrological similar pixels algorithm. Agricultural Water Management 267, 107602. https://doi.org/10.1016/j.agwat.2022.107602

Campbell, B.M., Beare, D.J., Bennett, E.M., Hall-Spencer, J.M., Ingram, J.S.I., Jaramillo, F., Ortiz, R., Ramankutty, N., Sayer, J.A., Shindell, D., 2017. Agriculture production as a major driver of the Earth system exceeding planetary boundaries. Ecology and Society 22.

Dari, J., Brocca, L., Quintana-Seguí, P., Escorihuela, M.J., Stefan, V., Morbidelli, R., 2020. Exploiting High-Resolution Remote Sensing Soil Moisture to Estimate Irrigation Water Amounts over a Mediterranean Region. Remote Sensing 12, 2593. https://doi.org/10.3390/rs12162593

Dari, J., Quintana-Seguí, P., Morbidelli, R., Saltalippi, C., Flammini, A., Giugliarelli, E., Escorihuela, M.J., Stefan, V., Brocca, L., 2022. Irrigation estimates from space: Implementation of different approaches to model

the evapotranspiration contribution within a soil-moisture-based inversion algorithm. Agricultural Water Management 265, 107537. https://doi.org/10.1016/j.agwat.2022.107537

Dari, J., Brocca, L., Modanesi, S., Massari, C., Tarpanelli, A., Barbetta, S., Quast, R., Vreugdenhil, M., Freeman, V., Barella-Ortiz, A., Quintana-Seguí, P., Bretreger, D., Volden, E., 2022. Regional data sets of high-resolution (1 and 6 km) irrigation estimates from space. https://doi.org/10.5281/zenodo.7341284

Dari, J., Brocca, L., Modanesi, S., Massari, C., Tarpanelli, A., Barbetta, S., Quast, R., Vreugdenhil, M., Freeman, V., Barella-Ortiz, A., Quintana Seguí, P., Bretreger, D., Volden, E., 2023. Regional data sets of high-resolution (1 and 6 km) irrigation estimates from space. Earth System Science Data 15, 1555–1575. https://doi.org/10.5194/essd-15-1555-2023

Das, N.N., Entekhabi, D., Dunbar, R.S., Chaubell, M.J., Colliander, A., Yueh, S., Jagdhuber, T., Chen, F., Crow, W., O'Neill, P.E., Walker, J.P., Berg, A., Bosch, D.D., Caldwell, T., Cosh, M.H., Collins, C.H., Lopez-Baeza, E., Thibeault, M., 2019. The SMAP and Copernicus Sentinel 1A/B microwave active-passive high resolution surface soil moisture product. Remote Sensing of Environment 233, 111380. https://doi.org/10.1016/j.rse.2019.111380

El Hajj, M., Baghdadi, N., Zribi, M., Bazzi, H., 2017. Synergic Use of Sentinel-1 and Sentinel-2 Images for Operational Soil Moisture Mapping at High Spatial Resolution over Agricultural Areas. Remote Sensing 9, 1292. https://doi.org/10.3390/rs9121292

FAO, 2021. The state of the world 's land and water resources for food and agriculture Available online: accessed on https://www.fao.org/land-water/solaw2021/en/. (Accessed 5 June 2023)

Felfelani, F., Pokhrel, Y., Guan, K., Lawrence, D.M., 2018. Utilizing SMAP Soil Moisture Data to Constrain Irrigation in the Community Land Model. Geophysical Research Letters 45, 12,892-12,902. https://doi.org/10.1029/2018GL080870

Ferguson, C.R., Pan, M., Oki, T., 2018. The Effect of Global Warming on Future Water Availability: CMIP5 Synthesis. Water Resources Research 54, 7791–7819. https://doi.org/10.1029/2018WR022792

Filippucci, P., Tarpanelli, A., Massari, C., Serafini, A., Strati, V., Alberi, M., Raptis, K.G.C., Mantovani, F., Brocca, L., 2020. Soil moisture as a potential variable for tracking and quantifying irrigation: A case study with proximal gamma-ray spectroscopy data. Advances in Water Resources 136, 103502. https://doi.org/10.1016/j.advwatres.2019.103502

Foley, J.A., Ramankutty, N., Brauman, K.A., Cassidy, E.S., Gerber, J.S., Johnston, M., Mueller, N.D., O'Connell, C., Ray, D.K., West, P.C., Balzer, C., Bennett, E.M., Carpenter, S.R., Hill, J., Monfreda, C., Polasky, S., Rockström, J., Sheehan, J., Siebert, S., Tilman, D., Zaks, D.P.M., 2011. Solutions for a cultivated planet. Nature 478, 337–342. https://doi.org/10.1038/nature10452

Foster, T., Mieno, T., Brozović, N., 2020. Satellite-Based Monitoring of Irrigation Water Use: Assessing Measurement Errors and Their Implications for Agricultural Water Management Policy. Water Resources Research 56, e2020WR028378. https://doi.org/10.1029/2020WR028378

Fritsch, F.N., Carlson, R.E., 1980. Monotone Piecewise Cubic Interpolation. SIAM J. Numer. Anal. 17, 238–246. https://doi.org/10.1137/0717021

Guzinski, R., Nieto, H., Sandholt, I., Karamitilios, G., 2020. Modelling High-Resolution Actual Evapotranspiration through Sentinel-2 and Sentinel-3 Data Fusion. Remote Sensing 12, 1433. https://doi.org/10.3390/rs12091433

Hengl, T., Jesus, J.M. de, Heuvelink, G.B.M., Gonzalez, M.R., Kilibarda, M., Blagotić, A., Shangguan, W., Wright, M.N., Geng, X., Bauer-Marschallinger, B., Guevara, M.A., Vargas, R., MacMillan, R.A., Batjes, N.H., Leenaars, J.G.B., Ribeiro, E., Wheeler, I., Mantel, S., Kempen, B., 2017. SoilGrids250m: Global gridded soil information based on machine learning. PLOS ONE 12, e0169748. https://doi.org/10.1371/journal.pone.0169748

Huang, Z., Hejazi, M., Li, X., Tang, Q., Vernon, C., Leng, G., Liu, Y., Döll, P., Eisner, S., Gerten, D., Hanasaki, N., Wada, Y., 2018. Reconstruction of global gridded monthly sectoral water withdrawals for 1971–2010 and analysis of their spatiotemporal patterns. Hydrology and Earth System Sciences 22, 2117–2133. https://doi.org/10.5194/hess-22-2117-2018

Jahn, R., Blume, H.P., Asio, V., Spaargaren, O., Schád, P., 2006. FAO Guidelines for Soil Description, 4th edition.

Jalilvand, E., Abolafia-Rosenzweig, R., Tajrishy, M., Das, N.N., 2021. Evaluation of SMAP/Sentinel 1 High-Resolution Soil Moisture Data to Detect Irrigation Over Agricultural Domain. IEEE Journal of Selected Topics in Applied Earth Observations and Remote Sensing 14, 10733–10747. https://doi.org/10.1109/JSTARS.2021.3119228

Jalilvand, E., Abolafia-Rosenzweig, R., Tajrishy, M., Kumar, S.V., Mohammadi, M.R., Das, N.N., 2023. Is It Possible to Quantify Irrigation Water-Use by Assimilating a High-Resolution Satellite Soil Moisture Product? Water Resources Research 59, e2022WR033342. https://doi.org/10.1029/2022WR033342

Jalilvand, E., Tajrishy, M., Ghazi Zadeh Hashemi, S.A., Brocca, L., 2019. Quantification of irrigation water using remote sensing of soil moisture in a semi-arid region. Remote Sensing of Environment 231, 111226. https://doi.org/10.1016/j.rse.2019.111226

Kerr, Y., Philippe, W., Wigneron, J.-P., Steven, D., Cabot, F., Jacqueline, B., Escorihuela, M.J., Font, J., Reul, N., Gruhier, C., Juglea, S., Drinkwater, M., Hahne, A., martin-neira, M., Susanne, M., 2010. The SMOS Mission: New Tool for Monitoring Key Elements of the Global Water Cycle. Proceedings of the IEEE 98. https://doi.org/10.1109/JPROC.2010.2043032

Koetz, B., Bastiaanssen, W., Berger, M., Defourney, P., Del Bello, U., Drusch, M., Drinkwater, M., Duca, R., Fernandez, V., Ghent, D., Guzinski, R., Hoogeveen, J., Hook, S., Lagouarde, J.-P., Lemoine, G., Manolis, I., Martimort, P., Masek, J., Massart, M., Notarnicola, C., Sobrino, J., Udelhoven, T., 2018. High Spatio-Temporal Resolution Land Surface Temperature Mission - a Copernicus Candidate Mission in Support of Agricultural Monitoring, in: IGARSS 2018 - 2018 IEEE International Geoscience and Remote Sensing Symposium. Presented at the IGARSS 2018 - 2018 IEEE International Geoscience and Remote Sensing Symposium, pp. 8160–8162. https://doi.org/10.1109/IGARSS.2018.8517433

Kumar, S.V., Peters-Lidard, C.D., Santanello, J.A., Reichle, R.H., Draper, C.S., Koster, R.D., Nearing, G., Jasinski, M.F., 2015. Evaluating the utility of satellite soil moisture retrievals over irrigated areas and the ability of land data assimilation methods to correct for unmodeled processes. Hydrology and Earth System Sciences 19, 4463–4478. https://doi.org/10.5194/hess-19-4463-2015

Laluet, P., Olivera-Guerra, L., Rivalland, V., Simonneaux, V., Inglada, J., Bellvert, J., Er-raki, S., Merlin, O., 2023a. A sensitivity analysis of a FAO-56 dual crop coefficient-based model under various field conditions. Environmental Modelling & Software 160, 105608. https://doi.org/10.1016/j.envsoft.2022.105608

Laluet, P., Olivera-Guerra, L., Altés, V., Rivalland, V., Jeantet, A., Tournebize, J., Cenobio-Cruz, O., Barella-Ortiz, A., Quintana Seguí, P., Villar, J.M., Merlin, O., 2023b. Drainage assessment of irrigation districts: on the precision and accuracy of four parsimonious models. Preprint. https://doi.org/10.5194/egusphere-2023-543

Lawrence, D.M., Oleson, K.W., Flanner, M.G., Thornton, P.E., Swenson, S.C., Lawrence, P.J., Zeng, X., Yang, Z.-L., Levis, S., Sakaguchi, K., Bonan, G.B., Slater, A.G., 2011. Parameterization improvements and functional and structural advances in Version 4 of the Community Land Model. Journal of Advances in Modeling Earth Systems 3. https://doi.org/10.1029/2011MS00045

Lawston, P.M., Santanello Jr, J.A., Kumar, S.V., 2017. Irrigation Signals Detected From SMAP Soil Moisture Retrievals. Geophysical Research Letters 44, 11,860-11,867. https://doi.org/10.1002/2017GL075733

Le Page, M., Jarlan, L., El Hajj, M.M., Zribi, M., Baghdadi, N., Boone, A., 2020. Potential for the Detection of Irrigation Events on Maize Plots Using Sentinel-1 Soil Moisture Products. Remote Sensing 12, 1621. https://doi.org/10.3390/rs12101621

López Valencia, O.M., Johansen, K., Aragón Solorio, B.J.L., Li, T., Houborg, R., Malbeteau, Y., AlMashharawi, S., Altaf, M.U., Fallatah, E.M., Dasari, H.P., Hoteit, I., McCabe, M.F., 2020. Mapping groundwater abstractions from irrigated agriculture: big data, inverse modeling, and a satellite–model fusion approach. Hydrology and Earth System Sciences 24, 5251–5277. https://doi.org/10.5194/hess-24-5251-2020

Malek, K., Adam, J.C., Stöckle, C.O., Peters, R.T., 2018. Climate change reduces water availability for agriculture by decreasing non-evaporative irrigation losses. Journal of Hydrology 561, 444–460. https://doi.org/10.1016/j.jhydrol.2017.11.046

Massari, C., Modanesi, S., Dari, J., Gruber, A., De Lannoy, G.J.M., Girotto, M., Quintana-Seguí, P., Le Page, M., Jarlan, L., Zribi, M., Ouaadi, N., Vreugdenhil, M., Zappa, L., Dorigo, W., Wagner, W., Brombacher, J., Pelgrum, H., Jaquot, P., Freeman, V., Volden, E., Fernandez Prieto, D., Tarpanelli, A., Barbetta, S., Brocca, L., 2021. A Review of Irrigation Information Retrievals from Space and Their Utility for Users. Remote Sensing 13, 4112. https://doi.org/10.3390/rs13204112

Merlin, O., Escorihuela, M.J., Mayoral, M.A., Hagolle, O., Al Bitar, A., Kerr, Y., 2013. Self-calibrated evaporation-based disaggregation of SMOS soil moisture: An evaluation study at 3km and 100m resolution in Catalunya, Spain. Remote Sensing of Environment 130, 25–38. https://doi.org/10.1016/j.rse.2012.11.008

Merlin, O., Stefan, V.G., Amazirh, A., Chanzy, A., Ceschia, E., Er-Raki, S., Gentine, P., Tallec, T., Ezzahar, J., Bircher, S., Beringer, J., Khabba, S., 2016. Modeling soil evaporation efficiency in a range of soil and atmospheric conditions using a meta-analysis approach. Water Resources Research 52, 3663–3684. https://doi.org/10.1002/2015WR018233

Modanesi, S., Massari, C., Bechtold, M., Lievens, H., Tarpanelli, A., Brocca, L., Zappa, L., De Lannoy, G.J.M., 2022. Challenges and benefits of quantifying irrigation through the assimilation of Sentinel-1 backscatter observations into Noah-MP. Hydrology and Earth System Sciences 26, 4685–4706. https://doi.org/10.5194/hess-26-4685-2022

Moradkhani, H., Hsu, K.-L., Gupta, H., Sorooshian, S., 2005. Uncertainty assessment of hydrologic model states and parameters: Sequential data assimilation using the particle filter. Water Resources Research 41. https://doi.org/10.1029/2004WR003604

Nair, A.S., Indu, J., 2019. Improvement of land surface model simulations over India via data assimilation of satellite-based soil moisture products. Journal of Hydrology 573, 406–421. https://doi.org/10.1016/j.jhydrol.2019.03.088

Niu, G.-Y., Yang, Z.-L., Mitchell, K.E., Chen, F., Ek, M.B., Barlage, M., Kumar, A., Manning, K., Niyogi, D., Rosero, E., Tewari, M., Xia, Y., 2011. The community Noah land surface model with multiparameterization options (Noah-MP): 1. Model description and evaluation with local-scale measurements. Journal of Geophysical Research: Atmospheres 116. https://doi.org/10.1029/2010JD015139

OECD, 2015. Drying Wells, Rising Stakes: Towards Sustainable Agricultural Groundwater Use. Organisation for Economic Co-operation and Development, Paris.

Ojha, N., Merlin, O., Molero, B., Suere, C., Olivera-Guerra, L., Ait Hssaine, B., Amazirh, A., Al Bitar, A., Escorihuela, M.J., Er-Raki, S., 2019. Stepwise Disaggregation of SMAP Soil Moisture at 100 m Resolution Using Landsat-7/8 Data and a Varying Intermediate Resolution. Remote Sensing 11, 1863. https://doi.org/10.3390/rs11161863

Oleson, K., Lawrence, M., Bonan, B., Drewniak, B., Huang, M., Koven, D., Levis, S., Li, F., Riley, J., Subin, M., Swenson, S., Thornton, E., Bozbiyik, A., Fisher, R., Heald, L., Kluzek, E., Lamarque, J.-F., Lawrence, J., Leung, R., Lipscomb, W., Muszala, P., Ricciuto, M., Sacks, J., Sun, Y., Tang, J., Yang, Z.-L., 2013. Technical description of version 4.5 of the Community Land Model (CLM). https://doi.org/10.5065/D6RR1W7M

Olivera-Guerra, L.-E., Laluet, P., Altés, V., Ollivier, C., Pageot, Y., Paolini, G., Chavanon, E., Rivalland, V., Boulet, G., Villar, J.-M., Merlin, O., 2023. Modeling actual water use under different irrigation regimes at district scale: Application to the FAO-56 dual crop coefficient method. Agricultural Water Management 278, 108119. https://doi.org/10.1016/j.agwat.2022.108119

Ouaadi, N., Jarlan, L., Ezzahar, J., Zribi, M., Khabba, S., Bouras, E., Bousbih, S., Frison, P.-L., 2020. Monitoring of wheat crops using the backscattering coefficient and the interferometric coherence derived from Sentinel-1 in semi-arid areas. Remote Sensing of Environment 251, 112050. https://doi.org/10.1016/j.rse.2020.112050

Ouaadi, N., Jarlan, L., Khabba, S., Ezzahar, J., Le Page, M., Merlin, O., 2021. Irrigation Amounts and Timing Retrieval through Data Assimilation of Surface Soil Moisture into the FAO-56 Approach in the South Mediterranean Region. Remote Sensing 13, 2667. https://doi.org/10.3390/rs13142667

Ozdogan, M., Rodell, M., Beaudoing, H., Toll, D., 2010. Simulating the Effects of Irrigation over the United States in a Land Surface Model Based on Satellite-Derived Agricultural Data. Journal of Hydrometeorology - J HYDROMETEOROL 11. https://doi.org/10.1175/2009JHM1116.1

Paolini, G., Escorihuela, M.J., Bellvert, J., Merlin, O., 2022. Disaggregation of SMAP Soil Moisture at 20 m Resolution: Validation and Sub-Field Scale Analysis. Remote Sensing 14, 167. https://doi.org/10.3390/rs14010167

Peng, J., Albergel, C., Balenzano, A., Brocca, L., Cartus, O., Cosh, M.H., Crow, W.T., Dabrowska-Zielinska, K., Dadson, S., Davidson, M.W.J., de Rosnay, P., Dorigo, W., Gruber, A., Hagemann, S., Hirschi, M., Kerr, Y.H., Lovergine, F., Mahecha, M.D., Marzahn, P., Mattia, F., Musial, J.P., Preuschmann, S., Reichle, R.H., Satalino, G., Silgram, M., van Bodegom, P.M., Verhoest, N.E.C., Wagner, W., Walker, J.P., Wegmüller, U., Loew, A., 2021. A roadmap for high-resolution satellite soil moisture applications – confronting product characteristics with user requirements. Remote Sensing of Environment 252, 112162. https://doi.org/10.1016/j.rse.2020.112162

Pereira, L.S., Paredes, P., Hunsaker, D.J., López-Urrea, R., Jovanovic, N., 2021. Updates and advances to the FAO56 crop water requirements method. Agricultural Water Management 248, 106697. https://doi.org/10.1016/j.agwat.2020.106697

Poggio, L., de Sousa, L.M., Batjes, N.H., Heuvelink, G.B.M., Kempen, B., Ribeiro, E., Rossiter, D., 2021. SoilGrids 2.0: producing soil information for the globe with quantified spatial uncertainty. SOIL 7, 217–240. https://doi.org/10.5194/soil-7-217-2021

Puy, A., Borgonovo, E., Lo Piano, S., Levin, S.A., Saltelli, A., 2021. Irrigated areas drive irrigation water withdrawals. Nat Commun 12, 1–12. https://doi.org/10.1038/s41467-021-24508-8

Puy, A., Lankford, B., Meier, J., Kooij, S. van der, Saltelli, A., 2022a. Large variations in global irrigation withdrawals caused by uncertain irrigation efficiencies. Environ. Res. Lett. 17, 044014. https://doi.org/10.1088/1748-9326/ac5768

Puy, A., Sheikholeslami, R., Gupta, H., Hall, J., Lankford, B., Lo Piano, S., Meier, J., Pappenberger, F., Porporato, A., Vico, G., Saltelli, A., 2022b. The delusive accuracy of global irrigation water withdrawal estimates. Nature Communications 13. https://doi.org/10.1038/s41467-022-30731-8

Qin, Y., Mueller, N.D., Siebert, S., Jackson, R.B., AghaKouchak, A., Zimmerman, J.B., Tong, D., Hong, C., Davis, S.J., 2019. Flexibility and intensity of global water use. Nat Sustain 2, 515–523. https://doi.org/10.1038/s41893-019-0294-2

Reichle, R.H., Koster, R.D., 2004. Bias reduction in short records of satellite soil moisture. Geophysical Research Letters 31. https://doi.org/10.1029/2004GL020938

Romaguera, M., Krol, M.S., Salama, M.S., Su, Z., Hoekstra, A.Y., 2014. Application of a Remote Sensing Method for Estimating Monthly Blue Water Evapotranspiration in Irrigated Agriculture. Remote Sensing 6, 10033–10050. https://doi.org/10.3390/rs61010033

Román Dobarco, M., Cousin, I., Le Bas, C., Martin, M.P., 2019. Pedotransfer functions for predicting available water capacity in French soils, their applicability domain and associated uncertainty. Geoderma 336, 81–95. https://doi.org/10.1016/j.geoderma.2018.08.022

Saltelli, A., Bammer, G., Bruno, I., Charters, E., Di Fiore, M., Didier, E., Nelson Espeland, W., Kay, J., Lo Piano, S., Mayo, D., Pielke Jr, R., Portaluri, T., Porter, T.M., Puy, A., Rafols, I., Ravetz, J.R., Reinert, E., Sarewitz, D., Stark, P.B., Stirling, A., van der Sluijs, J., Vineis, P., 2020. Five ways to ensure that models serve society: a manifesto. Nature 582, 482–484. https://doi.org/10.1038/d41586-020-01812-9

Santoro, M., Beer, C., Cartus, O., Schmullius, C., Shvidenko, A., McCallum, I., Wegmüller, U., Wiesmann, A., 2011. Retrieval of growing stock volume in boreal forest using hyper-temporal series of Envisat ASAR ScanSAR backscatter measurements. Remote Sensing of Environment 115, 490–507. https://doi.org/10.1016/j.rse.2010.09.018

Simonneaux, V., Lepage, M., Helson, D., Metral, J., Thomas, S., Duchemin, B., Cherkaoui, M., Kharrou, H., Berjami, B., Chehbouni, A., 2009. Estimation spatialisée de l'évapotranspiration des cultures irriguées par

télédétection : application à la gestion de l'irrigation dans la plaine du Haouz (Marrakech, Maroc). Science et changements planétaires / Sécheresse 20, 123–130. https://doi.org/10.1684/sec.2009.0177

Tilman, D., Clark, M., 2015. Food, Agriculture & the Environment: Can We Feed the World & Save the Earth? Daedalus 144, 8–23. https://doi.org/10.1162/DAED_a_00350

van Leeuwen, P.J., Künsch, H.R., Nerger, L., Potthast, R., Reich, S., 2019. Particle filters for high-dimensional geoscience applications: A review. Quarterly Journal of the Royal Meteorological Society 145, 2335–2365. https://doi.org/10.1002/qj.3551

Vogels, M.F.A., de Jong, S.M., Sterk, G., Wanders, N., Bierkens, M.F.P., Addink, E.A., 2020. An object-based image analysis approach to assess irrigation-water consumption from MODIS products in Ethiopia. International Journal of Applied Earth Observation and Geoinformation 88, 102067. https://doi.org/10.1016/j.jag.2020.102067

Vrugt, J.A., ter Braak, C.J.F., Diks, C.G.H., Schoups, G., 2013. Hydrologic data assimilation using particle Markov chain Monte Carlo simulation: Theory, concepts and applications. Advances in Water Resources, 35th Year Anniversary Issue 51, 457–478. https://doi.org/10.1016/j.advwatres.2012.04.002

Wada, Y., Flörke, M., Hanasaki, N., Eisner, S., Fischer, G., Tramberend, S., Satoh, Y., van Vliet, M.T.H., Yillia, P., Ringler, C., Burek, P., Wiberg, D., 2016. Modeling global water use for the 21st century: the Water Futures and Solutions (WFaS) initiative and its approaches. Geoscientific Model Development 9, 175–222. https://doi.org/10.5194/gmd-9-175-2016

Wada, Y., van Beek, L.P.H., Viviroli, D., Dürr, H.H., Weingartner, R., Bierkens, M.F.P., 2011. Global monthly water stress: 2. Water demand and severity of water stress. Water Resources Research 47. https://doi.org/10.1029/2010WR009792

Wada, Y., Wisser, D., Eisner, S., Flörke, M., Gerten, D., Haddeland, I., Hanasaki, N., Masaki, Y., Portmann, F.T., Stacke, T., Tessler, Z., Schewe, J., 2013. Multimodel projections and uncertainties of irrigation water demand under climate change. Geophysical Research Letters 40, 4626–4632. https://doi.org/10.1002/grl.50686

Zappa, L., Schlaffer, S., Bauer-Marschallinger, B., Nendel, C., Zimmerman, B., Dorigo, W., 2021. Detection and Quantification of Irrigation Water Amounts at 500 m Using Sentinel-1 Surface Soil Moisture. Remote Sensing 13, 1727. https://doi.org/10.3390/rs13091727

Zappa, L., Schlaffer, S., Brocca, L., Vreugdenhil, M., Nendel, C., Dorigo, W., 2022. How accurately can we retrieve irrigation timing and water amounts from (satellite) soil moisture? International Journal of Applied Earth Observation and Geoinformation 113, 102979. https://doi.org/10.1016/j.jag.2022.102979